

(NASA-CR-148512) . MELTING BEHAVIOR AND PHASE RELATIONS OF LUNAR SAMPLES Semiannual Progress Report, 1 Feb. - 31 Jul. 1976 (Harvard Univ.) . 74 p HC \$4.50	N76-29144
CSSL 03B	Unclas 63/91 47632

Progress Report to
 NATIONAL AERONAUTICS AND SPACE ADMINISTRATION
 Summarizing progress of research on
 MELTING BEHAVIOR AND PHASE RELATIONS
 OF LUNAR SAMPLES
 carried out under
 NGL 22-007-247

Principal Investigator: James Fred Hays
 Professor of Geology
 Hoffman Laboratory
 Harvard University
 Cambridge, MA 02138

~~Semiannual Progress Report, 1 August 1975 - 31 January 1976~~
 and
 Semiannual Progress Report, 1 February 1976 - 31 July 1976

REPRODUCTION RESTRICTIONS OVERRIDDEN
 NASA Scientific and Technical Information Facility



HARVARD UNIVERSITY
DEPARTMENT OF GEOLOGICAL SCIENCES

BERNHARD KUMMEL, *Chairman*

ULRICH PETERSEN,

Counsellor for Graduate Students

JAMES F. HAYS,

Counsellor for Undergraduate Students

HOFFMAN LABORATORY, 20 OXFORD STREET
CAMBRIDGE, MASSACHUSETTS 02138

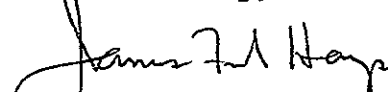
10 August 1976

NASA Scientific and Technical Information Facility
Post Office Box 8757
Baltimore/Washington International Airport
Baltimore MD 21240

Gentlemen:

Enclosed are two copies each of the Interim Progress Reports for NASA grant NGL 22-007-247. Also enclosed are reprints of several published papers giving results of this research.

Yours truly,



James Fred Hays
Professor of Geology

JFH:ci

PROGRESS REPORT

This report summarizes research carried out at Harvard University under NASA grant NGL 22-007-247 during the report periods 1 August 1975 through 31 January 1976 and 1 February 1976 through 31 July 1976. During this period eight papers have been published or accepted for publication; five of these were written during the previous reporting period and three papers report new work completed this year. In addition, nine talks on lunar research were given at professional meetings; all but one were published in abstract form.

During this report year our research has followed generally the lines set forth in last year's report and proposal. The cooling rate studies described in the earlier report have now been applied to the Apollo 12 mare basalt suite in an attempt to deduce the geometry of the flow or flows from which they came. This involved using the experimental data on crystallization history and liquid compositions to calculate liquid viscosities and densities as a function of time, then making model calculations of crystal settling during cooling of a magma body, and comparing the results obtained with observations on the Apollo 12 samples. We conclude that the samples studied came from near the bottom of a rather thick flow. This work is described in paper 7 (preprint attached).

Study of titaniferous basalt samples 74275 and 70215 revealed a significant degree of heterogeneity within each of these rocks in terms of major - as well as minor - element composition. The reason for this heterogeneity is not yet fully understood, but it must be taken into account in discussions of the origin of these rocks. We have shown that the observed heterogeneity is sufficient

to account for the apparent conflicts between the experimental crystallization data on these two samples, and that the existence of this heterogeneity severely limits our ability to determine the depth-of-origin from phase-equilibrium data. See paper 6 (reprint attached) for details.

Our efforts to codify and summarize the very large amount of chemical data on experimental run products continue. The relationship between Fe and Mg in olivine and coexisting liquid was described last year, generally confirming the earlier results of Røedder and Emslie who used terrestrial materials. This year John Longhi completed a lengthy study of Fe and Mg in plagioclase and the related problem of stoichiometry in lunar plagioclase. The essence of this work with lunar applications is reported in paper 8 and abstract 6 (preprints enclosed). Further details are in Longhi's Ph.D. thesis.

During the course of the year, Walker designed and built a molybdenum strip furnace for the melting of rock samples to facilitate XRF and microprobe analysis for major and minor element bulk compositions. Although this apparatus was not intended to be used with lunar samples, some interesting lunar applications have been found. For example, it was easy to show that calcic plagioclase readily floats in a synthetic melt with a composition matching that of the liquid from which lunar crustal plagioclase is believed to have crystallized. This puts to rest a question that has been hotly debated (see abstract 9, attached).

Furthermore, with the strip furnace it may be possible to obtain heats of fusion for lunar rocks or their analogs. Such data is needed for many purposes, and is almost totally lacking for terrestrial as well as lunar rocks. Work is in progress to develop and prove out the technique.

John Longhi received his Ph.D. degree in June 1976 and is now a Postdoctoral Research Fellow at MIT. Edward Stolper has received his M.Phil. degree from the University of Edinburgh for his thesis on the experimental petrology and origin of basaltic achondrites and will return to Harvard in September to rejoin the lunar group here.

PERSONNEL

James Fred Hays Professor of Geology	Principal Investigator
David Walker Research Fellow	Co-Investigator
John Longhi Graduate Student	Research Assistant
Nicholas Darbois Graduate Student	Research Assistant
Anthony Anastasio	Machinist
Kenneth Vidato	Machinist's helper

PUBLICATIONS
(1 August 1975 - 31 July 1976)

Articles in Books or Scientific Journals

1. Lunar igneous rocks and the nature of the lunar interior. J.F. Hays and D. Walker. Proc. Soviet-American Conf. on Cosmochemistry of the Moon and Planets, Moscow. The Lunar Science Institute (in press).
2. Origin of titaniferous lunar basalts. D. Walker, J. Longhi, T.L. Grove, E.M. Stolper, and J.F. Hays. Geochim. Cosmochim. Acta, 39, 1219-1235, 1975.
3. Differentiation of a very thick magma body with implications for the source regions of mare basalts. D. Walker, J. Longhi, and J.F. Hays. Proc. Sixth Lunar Sci. Conf., Geochim. Cosmochim. Acta, Suppl. 6, 1103-1120, 1975.
4. Crystallization history of lunar picritic basalt sample 12002: phase-equilibria and cooling rate studies. D. Walker, R.J. Kirkpatrick, J. Longhi, and J.F. Hays. Geol. Soc. Amer. Bull., 87, 646-656, 1976.
5. Direct determination of the quartz-coesite transition by in-situ x-ray measurements: a discussion. J.F. Hays. Contrib. Mineral. Petrol., 53, 61-63, 1975.
6. Heterogeneity in titaniferous lunar basalts. D. Walker, J. Longhi, and J.F. Hays. Earth Planet. Sci. Letters, 30, 27-36, 1976.

7. Differentiation of an Apollo 12 picrite magma. D. Walker, J. Longhi, R.J. Kirkpatrick, and J.F. Hays. Proc. Seventh Lunar Sci. Conf., Geochim. Cosmochim. Acta, Suppl. 7 (in press).
8. Fe and Mg in plagioclase. J. Longhi, D. Walker, and J.F. Hays. Proc. Seventh Lunar Sci. Conf., Geochim. Cosmochim. Acta, Suppl. 7 (in press).

Abstracts and Talks given at Meetings

1. Acceptance speech for F.W. Clarke Medal. D. Walker. *Geochim. Cosmochim. Acta*, 40, 567-569, 1976.
2. Heterogeneity in titaniferous lunar basalts. D. Walker, J. Longhi, and J.F. Hays. Origins of Mare Basalts, The Lunar Science Institute, Houston, Texas, 169-173, 1975.
3. Experimental petrology of mare basalts: an introduction. J.F. Hays. Given orally at Mare Basalt Conference, The Lunar Science Institute, Houston, Texas, November 1975.
4. Differentiation of a thin magma body. D. Walker, J. Longhi, and J.F. Hays. Lunar Science VII, 904-906, The Lunar Science Institute, Houston, Texas, 1976.
5. Fe, Mg, and silica in lunar plagioclase. J. Longhi, D. Walker, and J.F. Hays. Lunar Science VII, 501-503, The Lunar Science Institute, Houston, Texas, 1976.
6. Solid solution and phase equilibria on the join anorthite-silica. J. Longhi and J.F. Hays. *Trans. Am. Geophys. Un. (EOS)*, 57, 340, 1976.
7. Olivine nucleation in lunar basaltic melts in iron capsules. D. Walker, R.J. Kirkpatrick, J. Longhi, and J.F. Hays. *Trans. Am. Geophys. Un. (EOS)*, 57, 356, 1976.
8. Crystallization of basalts in the laboratory. J.F. Hays. *Geol. Soc. Amer. 1976 Ann. Meeting Rocky Mountain Section, Abstr. with Prog.* 8, 590, 1976.

9. Feldspar flotation and lunar crust formation. D. Walker and J.F. Hays. (submitted for presentation at Geol. Soc. Amer. 1976 Ann. Meeting).

REPRINTS AND PREPRINTS

Heterogeneity in titaniferous lunar basalts.

Differentiation of an Apollo 12 picrite magma.

Fe and Mg in Plagioclase.

Solid solution and phase equilibria on the join
anorthite-silica (abstract).

Feldspar flotation and lunar crust formation (abstract).

[6]

HETEROGENEITY IN TITANIFEROUS LUNAR BASALTS

DAVID WALKER, JOHN LONGHI and JAMES F. HAYS

*Hoffman Laboratory, Center for Earth and Planetary Physics, Harvard University,
Cambridge, Mass. (USA)*

Received December 12, 1975

Revised version received January 28, 1976

Small, but real, chemical differences exist between subsamples of fine-grained, quench-textured titaniferous lunar basalts. The existence of different textural domains with different chemistries is thought to account for most of this variation. In addition to the textural domains, 74275 has a population of a few percent of $Fe_{77.80}$ olivine "megacrysts", as well as dunite fragments of $Fe_{80.84}$. These materials are thought to be extraneous and to compromise the primary nature of 74275.

Recognition of the small chemical variations present may aid in understanding some discrepancies in the experimental petrology literature. However, these small variations have a distressing petrogenetic significance since they severely limit resolution in recognizing the number and depth of origin of primary magmas.

1. Introduction

Titaniferous lunar basalts returned from the Apollo 11 and 17 landing sites have proved to be a continuing subject of controversy in lunar petrogenesis. Originally the Apollo 11 basalts were interpreted on the basis of experimental petrology either as extreme residues of fractional crystallization near the lunar surface [1] or as incipient melts of the primitive lunar interior [2]. An alternative interpretation based on trace element studies [3] was that the titaniferous basalts represented the melting products of evolved regions of the lunar interior. The study of fine-grained, igneous textured titaniferous basalts from Apollo 17, which could not be explained as the residue of near-surface fractional crystallization, produced experimental evidence that the parental titaniferous basalts could be produced at relatively shallow depths (100–150 km) in the moon by melting of an ilmenite-bearing source region [4,5]. This evidence supported the interpretation of melting of cumulates and was consistent with the idea that the moon had been melted to a depth of at least a few hundred kilometers very early in its history and had differentiated into a series of floating and sinking cumulate layers [6–9]. In this model the mare basalts

are derived as the melting product of the sunken mafic cumulates. The principle difference between low- and high-Ti basalts is that the high-Ti basalts are derived from shallower depths by melting of the last formed, most differentiated cumulates whereas the low-Ti basalts have their source regions in the deeper, earlier cumulates.

This interpretation of the high-Ti mare basalts is based on finding ilmenite, olivine, and clinopyroxene on the liquidus of 70215, a fine-grained igneous sample, at between 5 and 7.5 kbar. This interpretation has been challenged [10] on the basis that 70215 is not the best representative of parental high-Ti basalt. 74275 with its higher Mg value ($100 \times Mg/Mg + Fe$ molar) and more olivine-normative character was alternatively proposed [10] as a parental high-Ti magma. Since 74275 had a higher pressure of olivine and pyroxene co-saturation (12 kbar) and since ilmenite is not also a saturating phase, the incentive for generating high- and low-Ti basalts from different source regions at different depths was greatly reduced.

It is the purpose of this paper to show that 70215 and 74275 are not so dissimilar as the previous studies suggest [4,10]; that the small differences result from sample heterogeneity coupled with minor olivine accu-

mulation; and that, while recognition of the differences can account for supposed experimental discrepancies, the differences are not sufficient to require drastic changes to existing models for the petrogenesis of high-Ti basalts

2. Textural domains and chemical variations

Rocks 70215 and 74275 are fine-grained rocks with petrographic characteristics indicating rapid crystallization from a silicate liquid. These characteristics include skeletal microphenocrysts, feathery to spherulitic crystal intergrowths, elaborate chemical zonation in minerals, and preservation of metastable armalcolite

and mesostasis glass in the solidification product. It was therefore assumed that the chemistries of both 70215 and 74275 represented the chemistries of liquids which existed at the surface of the moon and petrogenetic discussion proceeded on that assumption.

Subsequent analytical and experimental work have cast doubt on this assumption, inasmuch as significant chemical heterogeneities appear to exist among different subsamples of each rock [28,24]. Figs. 1 and 2 display the published analyses of subsamples of 70215 and 74275 [10-18]. These projections have proved to be useful in discussing the crystallization behavior of titaniferous lunar basalts [5]. It is clear that a range of compositions is present in both 70215 and 74275 and that the ranges are about the same size in each case.

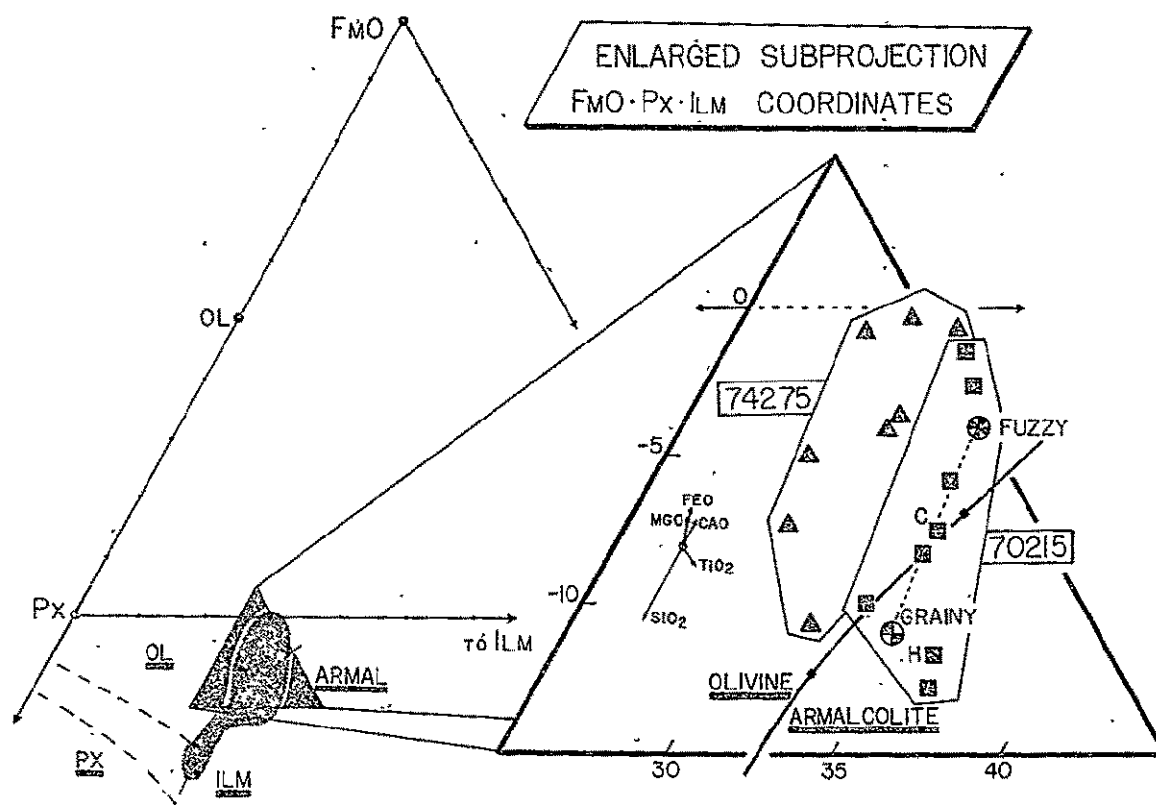


Fig. 1. Projection system for titaniferous basalt compositions used in fig. 2 of Walker et al. [5]. Underlined minerals are the liquid phases in that part of composition space. Shaded blob covers compositions of low-K, high-Ti basalts of Apollo 11 and 17. Enlarged triangle shows reported compositions of 70215 and 74275 [10-18]. Fuzzy and grainy are compositions of textural domains from Table 1. C and H are compositions of 70215 studied at Canberra [10] and Harvard [4]. Rosette of arrows indicates the magnitude and direction of displacement of compositions corresponding to the analytical precision of each oxide.

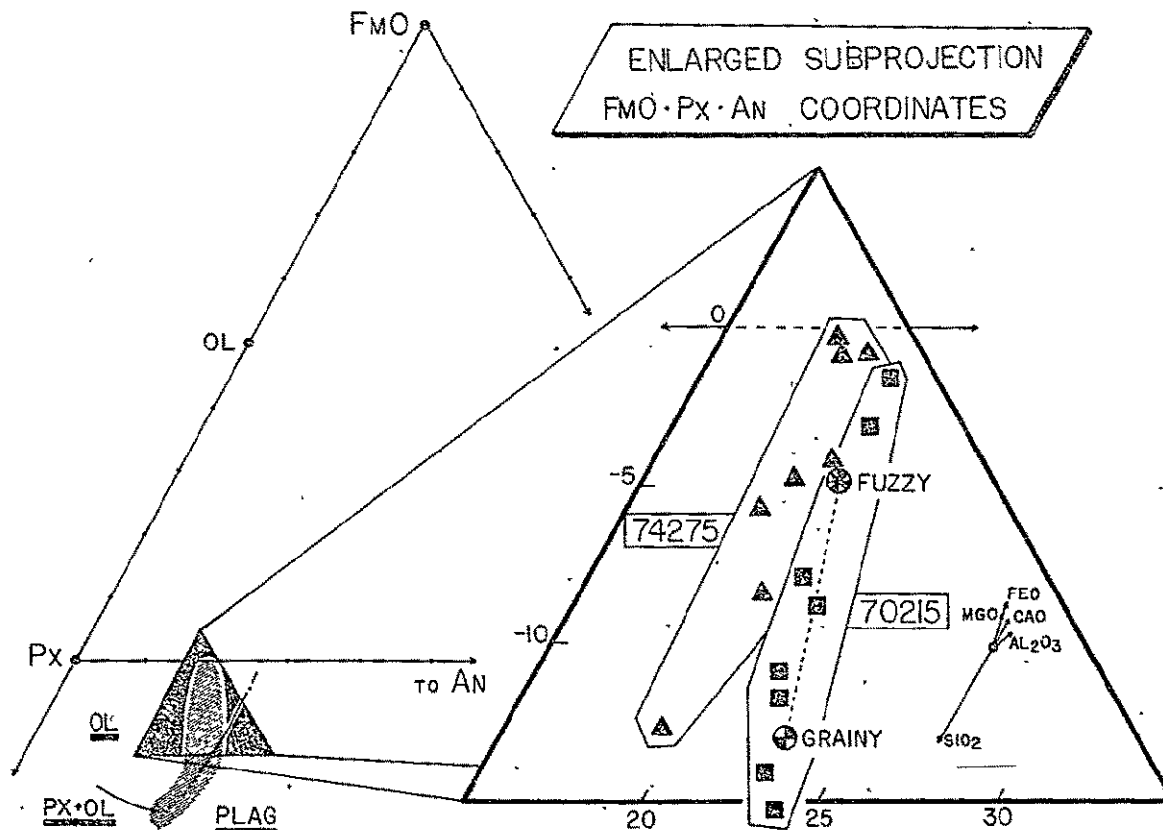


Fig. 2. Projection system for titaniferous basalt compositions from FmTiO_3 used in fig. 3 of Walker et al. [5]. Underlined minerals are the liquidus phases in that part of composition space. Shaded blob covers compositions of low-K, high-Ti basalts of Apollo 11 and 17. Enlarged triangle shows reported compositions of 70215 and 74275 [10–18]. Fuzzy and grainy are compositions of textural domains from Table 1. Rosette of arrows indicates the magnitude and direction of displacement of compositions corresponding to the analytical precision of each oxide.

The variations are actually rather small, however, they are significantly above the analytical precision (about a factor of 3). This is especially clear since two subsamples of 70215 were analyzed in the same laboratory by the same technique [16,17]. It is concluded that real chemical differences exist between subsamples of 70215 and 74275. Furthermore the differences cannot be the result of simple crystal settling or local fractional crystallization. The chemical variation does not conform to simple olivine or armalcolite fractionation curves. In Fig. 1 the cosaturation liquidus curve of olivine with armalcolite [4] cuts across the field of 70215. If the range in 70215 were caused by local fractional crystallization, the variation should follow

this liquidus boundary and *not* cross it.

How, then, do these chemical differences arise? Fig. 3A shows section 70215,147 to be texturally heterogeneous. Fig. 3B shows in an enlargement of 70215,147 that the textural domains differ principally in crystal morphology. The more translucent domain is characterized by better crystallized, slightly pink, granular pyroxene whereas the darker domain is characterized by more poorly crystallized spherulitic intergrowths of fuzzy-appearing pyroxene with the other minerals. These domains are dubbed “fuzzy” and “grainy” for convenient reference. Similar domains are found in 74275 as well as in other high-Ti Apollo 17 basalts (e.g. 71569, 72155, 72135). Fig. 3C shows

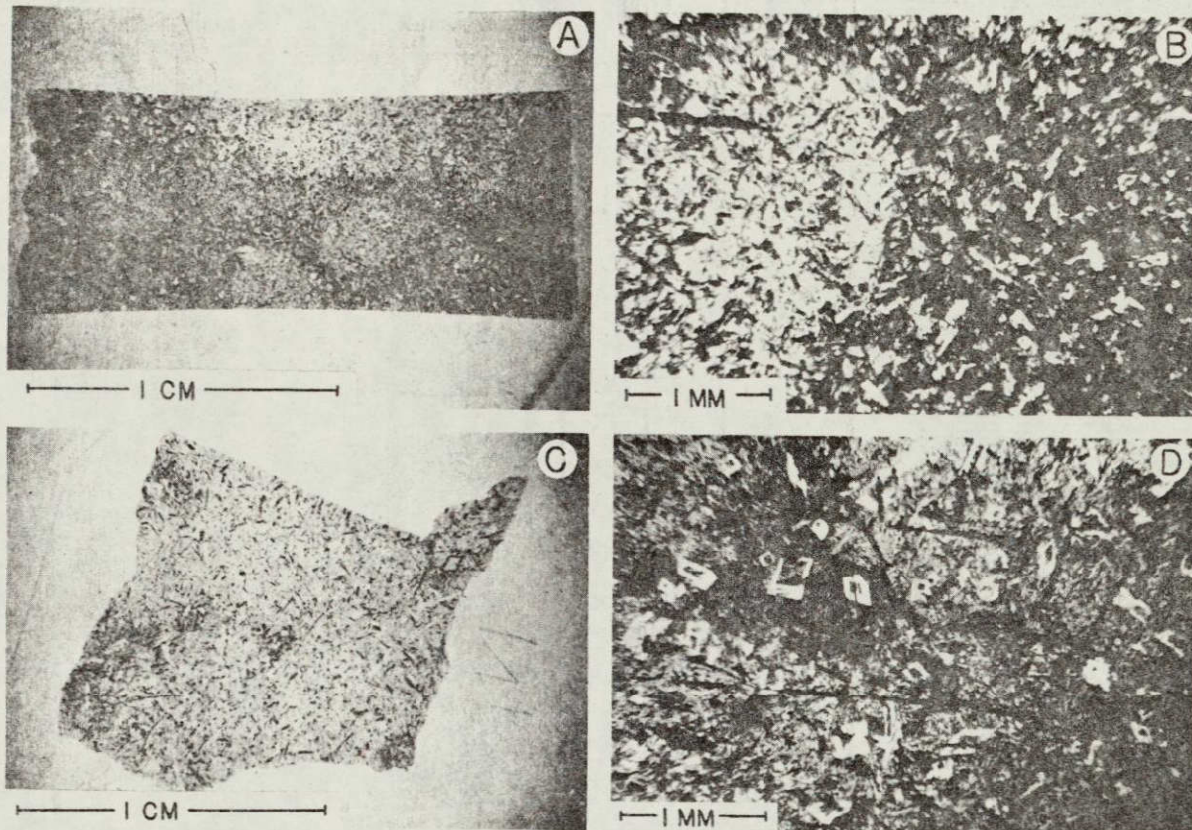


Fig. 3. A. 70215,147; transmitted light, note heterogeneous textural domains. B. 70215,147; enlargement of A. C. 70215,156; transmitted light. D. 70215,156; enlargement of C, note skeletal olivine microphenocrysts.

TABLE 1

Textural domain and olivine compositions

	70215,147 grainy *	70215,147 fuzzy *	74275,97 (a)	Olivines ** (b)	(c)
SiO ₂	38.0	37.2	38.8	38.8	37.7
TiO ₂	12.8	13.3	0.13	0.13	0.18
Al ₂ O ₃	9.2	8.6			
Cr ₂ O ₃			0.31	0.37	0.28
FeO	18.7	19.9	15.6	17.6	22.3
MgO	8.0	8.7	44.0	41.8	38.4
MnO			0.20	0.24	0.28
CaO	10.8	10.6	0.26	0.25	0.32
NiO			0.06	0.02	0.05
ZnO			0.02	0.17	0.21
	97.5	98.3	99.58	99.38	99.72

* Electron microprobe defocused beam partial analyses. Oxide percentages in each domain, after normal matrix correction procedures, were normalized to the average of published 70215 oxide values to correct for abnormal matrix effects inherent in defocused beam techniques applied to analysis of thin sections. Values used for 70215 average, grainy, and fuzzy are: SiO₂, 37.61, 43.2, 42.3; TiO₂, 13.05, 11.1, 11.5; Al₂O₃, 8.88, 12.7, 11.9; FeO, 19.34, 17.6, 18.7; MgO, 8.35, 7.6, 8.2; CaO, 10.69, 11.1, 10.9.

** (a) Core of "dunite" xenolith in Fig. 3H. (b) Core of large euhedral phenocryst. (c) Microphenocryst in groundmass.

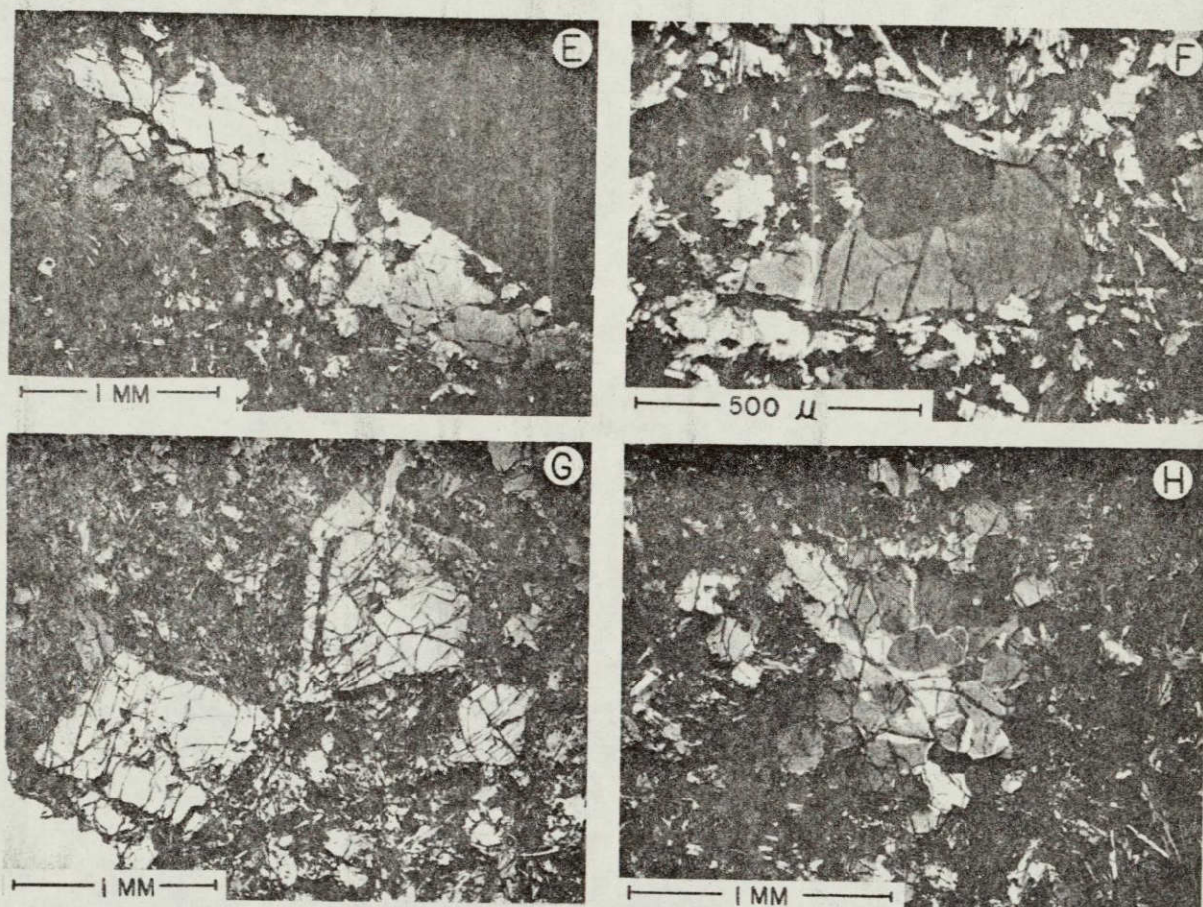


Fig. 3 (continued). E. 74275,94; transmitted light, crossed polarizers. Olivine "megacryst". F. 74275,94; transmitted light, crossed polarizers. Olivine xenolith. G. 74275,97; transmitted light. Large euhedral olivine crystals. H. 74275,97; transmitted light, crossed polarizers. Dunite xenolith with annealed granular texture.

that these domains are not small in comparison with a thin section (and therefore a subsample for analytical or experimental work) since 70215,156 is predominantly "grainy" domain texture. Defocused beam microprobe analysis was done on different domains in 70215,147 (see Table 1). The results are indicated in Figs. 1 and 2. The domains have measurably different chemistry and vary in the same sense as the range of compositions reported for the subsamples. Thus the inclusion of variable proportions of these domains in the subsamples appears to be capable of causing the compositional variation among the subsamples of a given rock. Although the reported subsamples show a slightly larger range in chemistry, it is thought that the

different textural domains occurring in different proportions explains much of the observed chemical variation between subsamples.

3. Origin of textural domains and implications

The origin of the textural domains is unknown. It is possible that the liquid was heterogeneous and that the different textures result from crystallization of parts of the liquid with different chemistry. This is considered to be extremely unlikely because textural differences appear to be much more strongly controlled by cooling history than by chemistry (compare

[19,20]) and the chemical differences are small. Furthermore, considering the ease with which these low-viscosity melts homogenize during laboratory fusion, it seems unreasonable to expect that heterogeneities could be maintained in the liquid for any appreciable time prior to solidification. This suggests that the heterogeneities are introduced *during* the solidification of a homogeneous liquid and requires that the material transfer rate within the solidifying magma exceeded the solidification rate. The need for some process to accomplish this objective has been anticipated in previous discussions of lunar basalt petrogenesis [21]. Briefly, the difference between the composition of plagioclase-saturated residual liquids and hand specimen compositions has been argued to result either from microphenocryst accumulation in the hand specimen (for which evidence is poor) or from some other unrecognized mass transfer process. In the present case it has been suggested that the granular areas may represent globules of solidified material which sank into material of slightly different composition which ultimately crystallized as the fuzzy textural domain [22]. The mass transfer distance might be characterized as "large" compared to a hand specimen.

Alternatively, it may be that the development of grainy and fuzzy areas is due to nucleation and growth effects under conditions of rapid cooling. It has been proposed [4] that early formed crystals nucleated and began to grow rapidly in isolated clusters with release of latent heat which locally reduced the cooling rate. This allowed pyroxene to nucleate before plagioclase and to coarsen, and permitted some olivine resorption. Between these clusters, nucleation of pyroxene was delayed until greater undercoolings were reached and the nucleation rate was much higher. As a result, when nucleation did take place, pyroxene and plagioclase together with ilmenite formed very fine radiate intergrowths, which now have a fuzzy appearance, and there was little opportunity for olivine resorption. Compositional variation among the domains results from the differential incorporation and exclusion of material as the clusters grew. Presumably there were compositional gradients in the melt between the clusters. In this model the mass transfer distance might be characterized as "small" compared to a hand specimen since material exchange occurs only on the scale of the domains.

Whatever the origin of these textural domains,

their demonstrated existence and chemical variation has several important implications. First it is fruitless to argue in detail about differences in experimental crystallization sequences and liquidus temperatures of allocated subsamples since these subsamples quite obviously are heterogeneous. In particular in Fig. 1, note that 70215 compositions cross the olivine-armalcolite liquidus boundary. Some subsamples should crystallize olivine first and some should crystallize armalcolite first, in iron capsules in a sealed tube. Composition H studied at Harvard [4] crystallizes armalcolite first and C studied at Canberra [10] crystallizes olivine, armalcolite (and spinel), at the liquidus. A synthetic composition was studied at Stony Brook [23] which crystallized both minerals simultaneously, although the reported mix did not lie exactly on the olivine-armalcolite curve shown here. It is thought that allocation heterogeneity may explain some of these experimental discrepancies. It should also be noted here that the large differences implied to exist between 74275 and 70215 [10] may not be so significant as thought. Such conclusions are strongly dependent on particular subsamples studies. The Mg number appears to be the major difference between the two samples, as will be discussed below.

Clearly subsamples of 70215 or 74275 may not represent liquid compositions as such, although they may have averages which were once liquids. Pieces of the same rock can be unrelatable to one another by normal crystal-liquid processes and might inspire a conclusion of a separate petrogenesis. Such a conclusion would be spurious. A similar state of affairs may also apply to some subsamples on which trace elements have been measured [24]. On the scale of investigation implied in sample allocation there is a danger of inferring more primary magmas than actually existed.

A final implication may be noted about the magnitude of chemical variation observed in the textural domains. They were small and we conclude that they result from mass transfer induced during solidification of a liquid. The scale of the mass transfer is not resolved and it could conceivably be large. Even if this is so, it must be noted that the variations documented are quite insufficient to explain the difference between hand specimens and cotectic liquid chemistry. Some additional mass transfer process would be required to explain the difference. We prefer to regard the cotectic liquids sampled (e.g. 75035) as products of fractional

crystallization of parental hand specimen compositions such as 70215 or 74275 since there is a continuous suite of hand specimen samples whose compositions follow a liquid line of descent from such parental compositions [4,5]. The compositional variation of the whole suite would require some rather improbable coincidences if they were to be interpreted as the products of crystal accumulation.

Note in Fig. 2 that the composition of the low-K, high-Ti basalt suite shows a *non-linear* pattern. It has been documented [4,5,10] that this "bent" pattern conforms to a liquid line of descent. It is difficult to see how this "bent" pattern could be produced during crystal accumulation in plagioclase-saturated liquids. Furthermore the accumulation model involving plagioclase-saturated liquids fails because the armalcolites actually found in the samples are not stable in pyroxene-plagioclase-saturated liquids [4,5,10,23]. We do not wish to preclude the possibility that some other mass transfer process may be operative, but crystal accumulation is highly improbable and whatever process leads to textural domain formation is quantitatively insufficient.

4. 70215 versus 74275

An additional feature of the petrography of 74275 needs discussion. Both 74275 and 70215 have skeletal microphenocrysts which occasionally are as large as 300 μm . See Fig. 3D. They are generally Fo_{77} or less magnesian. In contrast to any other high-Ti basalt thin sections we have seen, thin sections of 74275 have a distinctive population of olivine "megacrysts" which reach 3 mm in size (Fig. 3E). Their very irregular morphology suggests that they are not phenocrysts trapped in a chilled liquid. Furthermore this population has occasional "megacrysts" in which more than one crystal is present very much as if it were a small xenolithic fragment of an olivine-rich rock with annealed granular texture (Fig. 3F). It is thought, on textural grounds, that these "megacrysts" do not represent phenocrysts grown from a 74275 melt but rather are crystal fragments included in 74275. This population comprises only a few percent of 74275 and compositionally is relatively magnesian Fo_{77-80} . Section 74275.97 has some special features in addition to these anhedral "megacrysts" [29]. It contains

a few large (up to 1.5 mm) euhedral olivine crystals with cores as magnesian as Fo_{81} (Fig. 3G). Also present is a 1-mm polycrystalline olivine clast with annealed granular texture (Fig. 3H). Crystals in the center of the clast are Fo_{84} whereas those on the edge are as iron-rich as Fo_{74} . This clast is interpreted as a xenolith of dunite [29] which has suffered some Fe-Mg exchange with the melt along its margins.

74275 has been claimed to be significantly more primitive (higher Mg-value and more normative olivine) than 70215 [10]. We have noted above that the magnitude of the presumed difference between 70215 and 74275 is quite dependent on which subsamples are examined and that in Figs. 1 and 2 there is quite a close approach of some of the subsamples of the two. Unfortunately these projections suppress Fe-Mg variation so this must be displayed separately in Fig. 4. The range of published compositions does not overlap here, thus showing that 74275 and 70215 are indeed distinguishable on this basis. Also shown in Fig. 4 are curves for olivine-liquid distribution coefficients of Fe-Mg for $K_D = 0.26$ and 0.28 , which are thought to be relevant to the crystallization of these titaniferous

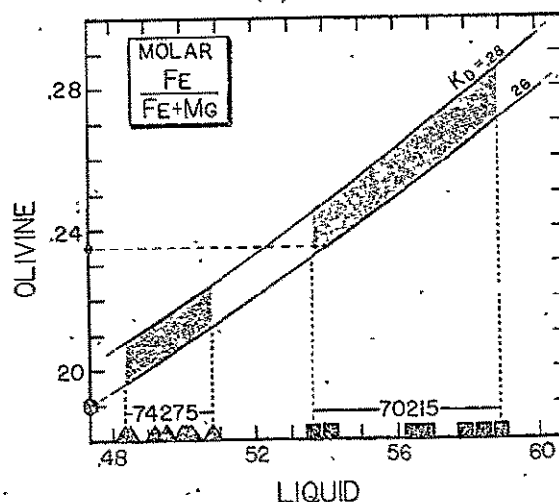


Fig. 4. Molar Fe/Fe + Mg of reported analyses of 70215 and 74275 [10-18]. Also plotted are Fe/Fe + Mg values of most magnesian olivines found in each sample. For 74275 this is taken to include the large euhedral olivines with phenocryst morphology (Fig. 3G) but does not include the Fo_{84} found in the dunite xenolith (Fig. 3H). Also shown are two olivine/liquid distribution coefficient curves for Fe/Mg [25,10].

lunar liquids [25,10]. It can be seen that within the precision of the data, the most magnesian olivines present in 70215 could have grown directly from liquids of 70215 composition. This does not appear to be true for 74275. Clearly the FO_{84} present in the dunite xenolith could not have grown from liquids of 74275 composition. The FO_{81} shown in Fig. 4 is for cores of large (millimeter size) euhedral olivines which have phenocryst morphology, however, it can be seen that even these are also too magnesian to be interpreted as the direct crystallization product of liquids of 74275 composition. Furthermore we questioned above on textural grounds whether the magnesian anhedral megacrysts in 74275 really do represent crystallization products of a 74275 liquid. We point out that exclusion of only 4% of such "megacrysts" from 74275 produces a composition with Mg value in the 70215 range. That is to say if 4% olivine megacrysts are added to a liquid with Mg value of 70215, the resultant mixture would have the higher Mg value and more normative olivine characteristic of 74275. This would require that the megacrysts and other peculiar olivines be xenocrysts from an unknown source, since olivines of this composition should not have grown from a liquid with 70215 Mg value. The xenocryst hypothesis appears to conform to some of the petrographic features of these peculiar olivines noted above.

We are not trying to prove that [olivine + 70215 = 74275] actually occurred since trace element characteristics seem to rule out such a direct relationship [23]. However, in view of the major element heterogeneities between subsamples, this hypothesis may not be impossible. Evaluation may critically depend on the choice of subsamples.

5. Petrogenetic discussion

A substantial part of the incentive for interpreting high-Ti basalt parental liquids (such as 70215) as the fusion product of Ti-enriched cumulates at relatively shallow depths within the moon was the discovery that 70215 was multiply saturated with olivine, pyroxene, and ilmenite at the liquidus at between 5 and 7.5 kbar [4]. This observation has been challenged [10] on the basis of experimental work on a different subsample of 70215. This work did not show multiple saturation with all three phases at 5 or 8 kbar although ilme-

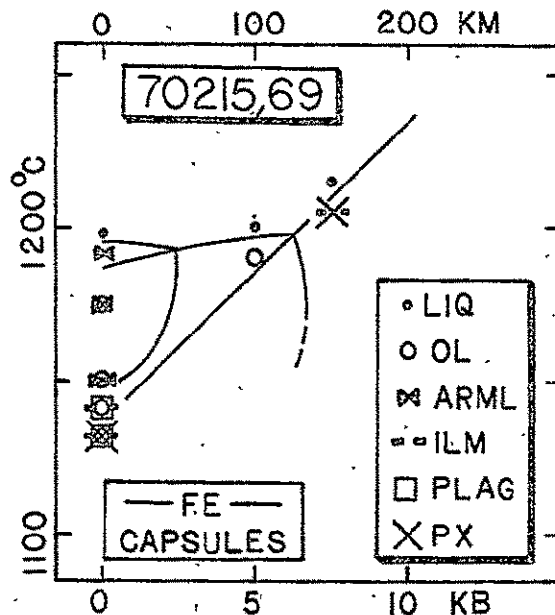


Fig. 5. Experimental results on 70215,69 as a function of pressure and temperature. All experiments in high-purity iron capsules. 70215,69 is saturated with olivine, pyroxene, and ilmenite between 5 and 7.5 kbar. Low-pressure crystallization from [4].

nite was close to olivine and pyroxene at 8 kbar. Even if the subsamples had the same chemistry, which they do not, it seems imprudent to us to challenge the original observation without making runs in the suggested pressure range between 5 and 7.5 kbar. We have performed new experiments in high-purity iron capsules to check our previous results in molybdenum and graphite [4] (see Fig. 5). At 1205°C and 7.5 kbar, 70215,69 is saturated with pyroxene and ilmenite less than 10°C from the liquidus; at 1190°C and 5 kbar, again less than 10°C from the liquidus, it is saturated with olivine alone. Spinel does not occur in this multiple saturation assemblage when Fe capsules are used. We feel that this confirms our earlier work showing that 70215,69 is saturated with olivine, pyroxene, and ilmenite at 6–7 kbar. Therefore, if 70215,69 is representative of a melt composition generated in the lunar interior, it may be interpreted as the melting product of an ilmenite-bearing source region at 100–150 km.

Since heterogeneities do exist between subsamples it is necessary to inquire how sensitive the multiple-

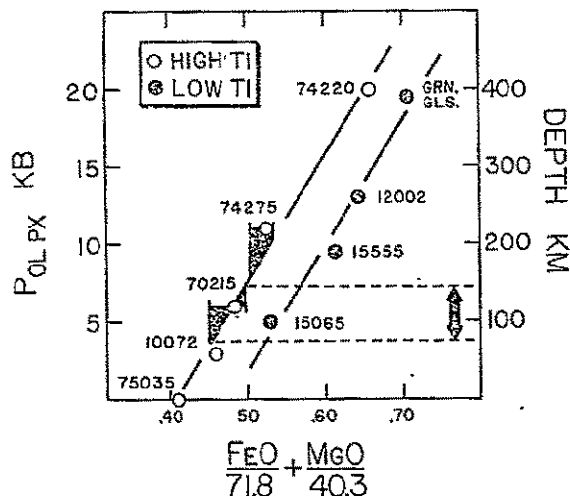


Fig. 6. $(\text{FeO}/71.8 + \text{MgO}/40.3)$ is plotted versus the liquidus cosaturation pressure of olivine and pyroxene for lunar basalt compositions. Data taken from references 4, 5, 10, 20, 26 and 27. Different lines with the same slope apply to high and low-Ti compositions. "Error bars" on 70215 and 74275 indicate the range in reported analyses. This variation causes an uncertainty of ~ 75 km in estimating the depth to olivine + pyroxene cosaturation for 70215.

saturation pressure (and hence depth-of-origin estimate) is to these small chemical variations. The pressure of cosaturation with pyroxene and olivine shows a regular dependence on the parameter $(\text{FeO}/71.8 + \text{MgO}/40.3)$ which is a measure of olivine abundance. Fig. 6 shows that different lines having the same slope apply to high-Ti and low-Ti lunar compositions. The variations in composition discussed above for 70215 and 74275 are indicated by the "error bars" in Fig. 6. Clearly the depth estimate is quite sensitive to these small chemical variations. The estimate for 70215 may vary by as much as 75 km based on the differences between subsamples alone! It is to be noted that if 4% "megacrysts" are removed from 74275 then the inferred depth of origin becomes the same as that of 70215, i.e. 100–150 km.

6. Summary

Perhaps it is pointless to argue in detail about which subsamples represent primary magmas, at what depth

they are generated, and how many are necessary. Certainly the factor of sample heterogeneity must be neutralized in some way before further progress can be made. How this is to be done with the present data base is unclear. However, at the present state of our investigations we can probably rule out "parental" samples such as 70215 as being products of crystal accumulation into cotectic liquids. If the "parental" compositions are in fact "primary" then the shallow-melting-of-Ti-rich-cumulates scenario follows. Rejection of this scenario, on the basis of results from 74275, is premature.

Acknowledgments

This work was supported by NASA Grant NGL 22-007-247 and the Committee on Experimental Geology and Geophysics of Harvard University. We thank S. Kesson for drawing our attention to the existence of the dunite clast in a section of 74275 we had not originally studied. We appreciate the comments of M.J. O'Hara and D.H. Green.

References

- 1 M.J. O'Hara, G.M. Biggar, S.W. Richardson, C.E. Ford and B.G. Jamieson, The nature of seas, mascons, and the lunar interior in the light of experimental studies, *Proc. Apollo 11 Lunar Sci. Conf., Geochim. Cosmochim. Acta, Suppl. 1, 1* (1970) 695–710.
- 2 A.E. Ringwood and E. Essene, Petrogenesis of the Apollo 11 basalts, internal constitution and origin of the moon, *Proc. Apollo 11 Lunar Sci. Conf., Geochim. Cosmochim. Acta, Suppl. 1, 1* (1970) 769–799.
- 3 J.A. Philpotts and C.C. Schnetzler, Apollo 11 lunar samples: K, Rb, Sr and rare-earth concentrations in some rocks and separated phases, *Proc. Apollo 11 Lunar Sci. Conf., Geochim. Cosmochim. Acta, Suppl. 1, 2* (1970) 1471–1486.
- 4 J. Longhi, D. Walker, T.L. Grove, E.M. Stolper and J.F. Hays, The petrology of the Apollo 17 mare basalts, *Proc. 5th Lunar Sci. Conf., Geochim. Cosmochim. Acta, Suppl. 5, 1* (1974) 447–469.
- 5 D. Walker, J. Longhi, E.M. Stolper, T.L. Grove and J.F. Hays, Origin of titaniferous lunar basalts, *Geochim. Cosmochim. Acta* 39 (1975) 1219–1235.
- 6 J.A. Wood, J.S. Dickey, U.B. Marvin and B.N. Powell, Lunar anorthosites and a geophysical model of the moon, *Proc. Apollo 11 Lunar Sci. Conf., Geochim. Cosmochim. Acta, Suppl. 1, 1* (1970) 965–988.

- 7 J.V. Smith, A.T. Anderson, R.C. Newton, E.J. Olsen, P.J. Wylie, A.V. Crewe, M.S. Isaacson and D. Johnson, Petrologic history of the moon inferred from petrography, mineralogy and petrogenesis of Apollo 11 rocks, Proc. Apollo 11 Lunar Sci. Conf., *Geochim. Cosmochim. Acta*, Suppl. 1, 1 (1970) 897–925.
- 8 S.R. Taylor and P. Jakes, The geochemical evolution of the moon, Proc. 5th Lunar Sci. Conf., *Geochim. Cosmochim. Acta*, Suppl. 5, 2 (1974) 1287–1305.
- 9 D. Walker, J. Longhi and J.F. Hays, Differentiation of a very thick magma body and implications for the source regions of mare basalts, Proc. 6th Lunar Sci. Conf., *Geochim. Cosmochim. Acta*, Suppl. 6, 1 (1975) in press.
- 10 D.H. Green, A.E. Ringwood, W.O. Hibberson and N.G. Ware, Experimental petrology of Apollo 17 mare basalts, Proc. 6th Lunar Sci. Conf., *Geochim. Cosmochim. Acta*, Suppl. 6 (1975) in press.
- 11 A.R. Duncan, A.J. Erlank, J.P. Willis, M.K. Sher and L.H. Ahrens, Trace element evidence for a two-stage origin of some titaniferous mare basalts, Proc. 5th Lunar Sci. Conf., *Geochim. Cosmochim. Acta*, Suppl. 5, 2 (1974) 1147–1157.
- 12 H.J. Rose, Jr., F. Cuttitta, S. Berman, F.W. Brown, M.K. Carron, R.P. Christian, E.J. Dwornik and L.P. Greenland, Chemical composition of rocks and soils at Taurus-Littrow, Proc. 5th Lunar Sci. Conf., *Geochim. Cosmochim. Acta*, Suppl. 5, 2 (1974) 1119–1133.
- 13 A.O. Brunfelt, K.S. Heier, B. Nilssen, E. Steinnes and B. Sundvoll, Elemental composition of Apollo 17 fines and rocks, Proc. 5th Lunar Sci. Conf., *Geochim. Cosmochim. Acta*, Suppl. 5, 2 (1974) 981–990.
- 14 M.D. Miller, R.A. Pacer, M.-S. Ma, B.R. Hawke, G.L. Lookhart and W.D. Ehmann, Compositional studies of the lunar regolith at the Apollo 17 site, Proc. 5th Lunar Sci. Conf., *Geochim. Cosmochim. Acta*, Suppl. 5, 2 (1974) 1079–1086.
- 15 H. Wanke, H. Palme, H. Baddenhausen, G. Dreibus, E. Jagoutz, H. Kruse, B. Spettel, F. Teschke and R. Thacker, Chemistry of Apollo 16 and 17 samples: bulk composition, late stage accumulation and early differentiation of the moon, Proc. 5th Lunar Sci. Conf., *Geochim. Cosmochim. Acta*, Suppl. 5, 2 (1974) 1307–1335.
- 16 LSPET, Apollo 17 lunar samples: chemical and petrographic description, *Science* 182 (1973) 659–672.
- 17 J.M. Rhodes, K.V. Rodgers, C. Shih, B.M. Bansal, L.E. Nyquist, H. Weismann and N.J. Hubbard, The relationship between geology and soil chemistry at the Apollo 17 landing site, Proc. 5th Lunar Sci. Conf., *Geochim. Cosmochim. Acta*, Suppl. 5, 2 (1974) 1097–1117.
- 18 H.J. Rose, Jr., R.P. Christian, E.J. Dwornik and M.M. Schnepfe, Major element analysis of some Apollo 15, 16, and 17 samples, in: *Lunar Science VI* (Lunar Science Institute, Houston, Texas, 1975) 686–688.
- 19 G. Lofgren, C.H. Donaldson, R.J. Williams, O. Mullins, Jr. and T.M. Usselman, Experimentally reproduced textures and mineral chemistry of Apollo 15 quartz normative basalts, Proc. 5th Lunar Sci. Conf., *Geochim. Cosmochim. Acta*, Suppl. 5, 1 (1974) 549–567.
- 20 D. Walker, R.J. Kirkpatrick, J. Longhi and J.F. Hays, Crystallization history of lunar picritic basalt 12002: phase equilibria and cooling rate studies, *Geol. Soc. Am. Bull.* (1976) in press.
- 21 M.J. O'Hara, G.M. Biggar, P.G. Hill, B. Jefferies and D. Humphries, Plagioclase saturation in lunar high-titanium basalt, *Earth Planet. Sci. Lett.* 21 (1974) 253–268; and M.J. O'Hara, personal communications (1973–1975).
- 22 M.J. O'Hara, personal communication (1975).
- 23 S.E. Kesson, Mare basalts: melting experiments and petrogenetic interpretations, Proc. 6th Lunar Sci. Conf., *Geochim. Cosmochim. Acta*, Suppl. 6, 1 (1975) in press.
- 24 C. Shih, L.A. Haskin, H. Weismann, B.M. Bansal and J.C. Brannon, On the origin of high-Ti mare basalts, Proc. 6th Lunar Sci. Conf., *Geochim. Cosmochim. Acta*, Suppl. 6, 2 (1975) in press.
- 25 J. Longhi, D. Walker and J.F. Hays, Fe–Mg distribution between olivine and lunar basaltic liquids, *EOS*, *Trans. Am. Geophys. Union* 56 (1975) 471.
- 26 J. Longhi, D. Walker, T.L. Grove, E.M. Stolper and J.F. Hays, Petrology and origin of Apollo 15 mare basalts (1975) in preparation.
- 27 E.M. Stolper, Lunar ultramafic glasses, Undergraduate Honors Thesis, Harvard University (1974).
- 28 M.J. O'Hara and D.J. Humphries, Analysis of compositional variations in high titanium basalts and related materials, in: *Lunar Science VI* (Lunar Science Institute, Houston, Texas, 1975) 616–618.
- 29 C.E. Meyer and H.G. Wishire, "Dunite" inclusion in lunar basalt 74275, in: *Lunar Science V* (Lunar Science Institute, Houston, Texas, 1974) 503–505.

Fe AND Mg IN PLAGIOCLASE

John Longhi,¹ David Walker² and James F. Hays²

Revised Version: May 28, 1976

Submitted to Proceedings of
7th Lunar Science Conference.¹Dept. of Earth and Planetary Sciences, Massachusetts Institute of Technology, Cambridge, Mass. 02139²Dept. of Geological Sciences, Harvard University, Cambridge, Mass. 02138Abstract

Distribution coefficients for Fe and Mg between plagioclase and basaltic liquids have been measured for lunar, terrestrial and synthetic systems. Observed substitution in plagioclase is consistent with a $\text{Ca}(\text{Fe},\text{Mg})\text{Si}_3\text{O}_8$ component, and Mg is incorporated into plagioclase more readily than ferrous iron. $K_{\text{P-L}}^{\text{Fe-Mg}} = 0.5$ for lunar basalts and synthetic analogs. As oxygen fugacity increases, ferric iron becomes significant and the bulk exchange coefficient $K_{\text{P-L}}^{\text{Fe}^{3+}\text{-Mg}}$ increases to an average of 1.4 for terrestrial basalts. The variation of $K_{\text{P-L}}^{\text{Fe}^{3+}\text{-Mg}}$ with oxygen fugacity provides a crude oxygen barometer. Lower concentrations of Fe and Mg in plagioclase from plutonic rocks suggest that crystallization kinetics significantly effect the observed distributions.

The new data imply that: 1) lunar anorthosites crystallized from relatively iron-rich liquids, 2) Fe/Mg zoning in plagioclase is an indicator of crystallization processes in basaltic magmas, 3) Fe/Mg heterogeneity in plagioclase is a clue to the recognition of impact melts.

Introduction

Although X^{Fe} ($= \frac{\text{Fe}}{\text{Fe} + \text{Mg}}$) in basaltic plagioclase was recognized as a potentially useful crystallization index (e.g., Longhi et al., 1972; Crawford, 1973), the detailed mechanisms of Fe and Mg substitution in plagioclase are debatable. Most chemical studies of lunar plagioclase indicate that nearly all deviations from Ab-Or-An chemistry can be explained by the components, $\text{Ca}(\text{Fe,Mg})\text{Si}_3\text{O}_8$ and $\square\text{Si}_4\text{O}_8$ (e.g., Weill et al., 1970; Wenk and Wilde, 1973) where \square signifies a Ca-site vacancy. Spectral studies (Hafner et al., 1971 and Appleman et al., 1972) indicate that much of the Fe is not situated in tetrahedral sites as would be expected from a $\text{Ca}(\text{Fe,Mg})\text{Si}_3\text{O}_8$ component, but appears to be situated in the larger, six- to eight-coordinated Ca-sites. Furthermore, Hafner et al. (1971) suggested that the Fe apparently in tetrahedral sites may be associated with oxygen vacancies. In order to predict the compositional dependence of Fe and Mg substitution it is necessary to know the dominant Fe-Mg component and also to model the effects of substitution on two types of sites.

Longhi et al. (1976), via projections in the system $\text{Ca}_4\text{Si}_2\text{O}_8\text{-Al}_8\text{Si}_2\text{O}_8\text{-Si}_4\text{O}_8\text{-(Fe,Mg)}_2\text{Si}_3\text{O}_8$, showed that all the chemical variation in plagioclase from mare basalts can be explained by mixing the conventional plagioclase components (An, Ab and Or) with $\square\text{Si}_4\text{O}_8$, $\text{Ca}(\text{Fe,Mg})\text{Si}_3\text{O}_8$ and $(\text{Fe,Mg})\text{Al}_2\text{Si}_2\text{O}_8$.

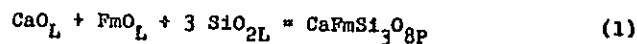
The data rule out any significant substitution of components involving oxygen vacancies (e.g., $\text{CaFm}_2\text{Si}_2\text{O}_7$), and also show that no more than about 10% of the Fe and Mg in plagioclase from mare basalts substitutes in the form of the $(\text{Fe,Mg})\text{Al}_2\text{Si}_2\text{O}_8$ component. Models of the multi-site crystal/single-site liquid equilibria (Longhi, 1976) based upon the analysis of Grover and Orville (1969) show that deviations from one-site/one-site equilibria will be obscured when the proportion of distinct sites in the multi-site phase is not 1:1. Thus in calcic plagioclase, where the proportion of sites available to Fe and Mg is likely to be 1(Ca):2(Al), Fe and Mg substitutions may effectively behave as if plagioclase had only a single type of available site.

We here examine the substitution of Fe and Mg in plagioclase as a function of composition and temperature, recognizing that the dominant component is $\text{Ca}(\text{Fe,Mg})\text{Si}_3\text{O}_8$. Possible pressure and kinetic effects will be considered.

Distribution Coefficients -- Theory

In order to deal with the compositional dependence of the distribution coefficients, we will assume that all the Fe^{+2} plus Mg forms a $\text{Ca}(\text{Fe},\text{Mg})\text{Si}_3\text{O}_8$ component in plagioclase.

Consider the reaction:



with equilibrium constant:

$$K_{\text{eq}}^{\text{Fm}} = \frac{[\text{CaFmSi}_3\text{O}_8]_P}{[\text{CaO}]_L \cdot [\text{FmO}]_L \cdot [\text{SiO}_2]_L^3} \quad (2)$$

where Fm denotes either Fe or Mg, subscripts P and L denote plagioclase and liquid respectively, and the brackets indicate activities. The conventional molar distribution coefficient is:

$$K_{P-L}^{\text{Fm}} = \frac{(\text{FmO})_P}{(\text{FmO})_L} = 0.2 K_{\text{eq}}^{\text{Fm}} [\text{CaO}]_L \cdot [\text{SiO}_2]_L^3 \cdot \gamma_L^{\text{FmO}} / \gamma_P^{\text{CaFmSi}_3\text{O}_8} \quad (3)$$

where 0.2 is the approximate stoichiometric factor for calcic plagioclase that relates FmO concentration to $\text{CaFmSi}_3\text{O}_8$ concentration when analyses are recalculated in terms of conventional oxides (i.e., Al_2O_3) and γ is an activity coefficient. Even if all the solutions were ideal mixtures of oxides the distribution coefficient would still vary as the concentration product, $(\text{CaO})_L \cdot (\text{SiO}_2)_L^3$. On the other hand, if most Fm substituted for Ca to form a $\text{FmAl}_2\text{Si}_2\text{O}_8$ component

then K_{P-L}^{Fm} would vary inversely with $(\text{Al}_2\text{O}_3)_L \cdot (\text{SiO}_2)_L^2$. We may predict that with decreasing Ca/Al in the melt, the proportion of Fm substitution for Ca will increase.

The direct composition dependence of simple distribution coefficients may be circumvented by the use of exchange distribution coefficients such as:

$$K_{P-L}^{\text{Fe-Mg}} = \frac{(\text{FeO})_P \cdot (\text{MgO})_L}{(\text{MgO})_P \cdot (\text{FeO})_L} = \frac{K_{P-L}^{\text{Fe}}}{K_{P-L}^{\text{Mg}}} \\ = \frac{K_{\text{eq}}^{\text{Fe}}}{K_{\text{eq}}^{\text{Mg}}} \cdot \frac{\gamma_L^{\text{FeO}}}{\gamma_L^{\text{MgO}}} \cdot \frac{\gamma_P^{\text{CaMgSi}_3\text{O}_8}}{\gamma_P^{\text{CaFeSi}_3\text{O}_8}} \quad (4)$$

Here the division cancels out the activity terms in equation (3). It can be readily shown that:

$$K_{P-L}^{\text{Fe-Mg}} = \frac{x_P^{\text{Fe}} \cdot (1-x_L^{\text{Fe}})}{(1-x_P^{\text{Fe}}) \cdot x_L^{\text{Fe}}} \quad (5)$$

where $x^{\text{Fe}} \equiv \text{Fe}/(\text{Fe} + \text{Mg})$. Thus it is possible to relate x_P^{Fe} to x_L^{Fe} by means of a single coefficient over a wide range of liquid composition. Given the formulation of plagioclase activities in terms of phase components, the activity coefficients $\gamma_P^{\text{CaFeSi}_3\text{O}_8}$ and $\gamma_P^{\text{CaMgSi}_3\text{O}_8}$ will probably vary with the An/Ab ratio. Because of the division in equation (4), the exchange coefficient, $K_{P-L}^{\text{Fe-Mg}}$, will be less sensitive to An/Ab variation than the single element coefficients.

An alternative approach to avoiding composition dependence

is to define more complex, single-element distribution coefficients that explicitly vary with liquid composition (Drake and Weill, 1975) such as

$$K_{P-L}^{Fe^+} = \frac{(FeO)_P}{[CaO]_L \cdot [FeO]_L \cdot ([SiO_2]_L)^3} \quad (6)$$

Several options are available for approximating liquid component activities by assuming ideal solutions: 1) ideal oxide mixing (activity equals concentration); 2) mixing of ions or oxides on two separate lattices (Temkin, 1945); or 3) separate mixing among network-forming and network-modifying components (Bottlinga and Weill, 1972). Although component activity approximations based upon the Bottlinga-Weill melt model seem to have the greatest potential utility, these approximations can be used only with liquids with restricted ranges of composition because the rigid, norm-like calculation of the proportions of melt species leads to unreal discontinuities in the distribution coefficients. For example, in an alkali-free liquid, if $(CaO)_L = (Al_2O_3)_L$ then $[CaO]_L = 0$ and $K_{P-L}^{Fe^+} = \infty$. Therefore, we will adopt the Temkin-melt model as a tentative basis for activity approximations and calculate activities as follows:

large cations (Fe, Mg, Ca, Cr, Ti, Na, K) --

$$[FeO]_L^* = \left(\frac{Fe}{Fe + Mg + Ca + Na + K + Ti + Cr} \right)_L \quad (7)$$

etc., and tetrahedrally coordinated ions (Si, Al) --

$$[SiO_2]_L^* = \left(\frac{Si}{Si + Al} \right)_L \quad (8)$$

where * signifies the Temkin model.

Experimental Techniques

All analyses were made with an ARL EMX-SM 120000 electron microprobe at 15kv, 0.011 to 0.015 μ A sample current and a 1-2 μ m wide beam. Synthetic, crystalline anorthite was the major element standard for Ca, Si and Al and as the background standard for Na, K, Fe, Mg and Ti. Typically, approximately 1,000 counts were accumulated for Fe and Mg, giving a counting error of ± 0.03 mole % FeO and MgO. Relative counting errors for Ca, Si and Al were $< \pm 1\%$.

Whenever the point of an analysis on plagioclase was closer than 50 μ m from a boundary with an iron-bearing phase a correction was made for secondary fluorescence of iron according to the empirical relation:

$$C_{An}^{Fe} / C_{\phi 2}^{Fe} = I_{An}^{Fe} / I_{\phi 2}^{Fe} = 0.011 \exp(-0.037x),$$

determined by Longhi (1976) where C_{An}^{Fe} is the apparent concentration of Fe in anorthite, I is x-ray intensity, $\phi 2$ refers to the iron-rich phase at x μ m from the point of analysis. Due to the cubic dependence of secondary fluorescence upon atomic number (Smith, 1965), the effect for magnesium is negligible. Most corrections were in the range 0.05 to 0.20 mole % FeO. No analysis was performed upon crystals with minimum dimensions < 10 μ m.

Fourteen glasses with compositions similar to those of lunar basaltic liquids saturated with plagioclase were synthesized from reagent grade oxides and Amelia albite by multiple fusions in platinum crucibles under a 95%N₂ / 5% H₂

atmosphere. After each fusion the sample was ground to a fine powder in a tungsten-carbide ball mill. The compositions spanned a range of atomic Fe/(Fe + Mg) from 0.2 to 0.8 and were chosen so that plagioclase was the sole liquidus phase, the liquidus temperature was approximately 1200°C, and the concentration of TiO₂ was approximately 1 wt%.

Experimental charges were loaded into high-purity iron capsules (Walker *et al.*, 1976) enclosed in sealed, evacuated silica tubes. The silica tubes were suspended in a Deltec T31 furnace with MoSi₂ elements and dropped into water at the end of the experiments. The charges were held ~20°C above the liquidus for a minimum of 48 hours to ensure equilibration with the iron capsules, then the temperature was lowered five to twenty degrees below the liquidus in one-half hour and held at constant temperature for a minimum of one week. This technique allows plagioclase crystals to grow with minimum dimensions > 10 μm and to approach equilibrium with the melt (Drake and Weill, 1975).

Experimental products of the seven compositions containing alkalis were plagued by the presence of iron spherules included in the plagioclase. Because of the uncertainties involved in applying corrections for secondary fluorescence, the data for these experiments (Longhi, 1976) are not included in the present discussion, although the distribution coefficients for iron and magnesium are similar to those obtained from the alkali-free compositions.

A series of five runs of variable length were made at 1230°C with a single composition, DFC.8, in order to test for possible iron gain as a result of oxygen diffusion through the silica glass tubing (Kesson, 1975). There was approximately 0.5 wt% FeO gain in the first 48 hours, but no measurable variation from 48 to 240 hours. Thus oxygen diffusion is not a factor in these experiments. However, changes in the composition of the melt as it equilibrates with the capsule are a potential source of serious error in short term experiments.

Crystal-Liquid Distribution

The distribution of iron and magnesium between plagioclase and liquid can be measured directly by microprobe analysis of quenched natural and synthetic crystal-liquid pairs. Indirect information from crystalline rocks can be obtained by comparing Fe and Mg concentrations in the cores of the earliest-formed plagioclase crystals with the estimated composition of coexisting liquid. If plagioclase was a liquidus phase of a quickly cooled melt, then the bulk rock composition represents the coexisting liquid composition (e.g., 68415, 14310, 12038, 75035). If plagioclase crystallized late, then the coexisting liquid composition may be estimated from melting experiments if the rock has cooled slowly (e.g., 15065, 15555 and 70017). Finally, if the rock has homogeneous minerals (e.g., pink-spinel and troctolite) then the FeO and MgO concentrations in the coexisting liquid can be calculated from olivine compositions if approximate temperatures are known (e.g., Roeder and Emslie, 1970).

Tables 1 and 2 contain direct data on eleven sets of synthetic and eight sets of natural plagioclase liquid pairs. The natural samples include submarine basalt glasses and glasses from Makaopuhi lava lake (Hawaii). Estimates of liquid composition are made for eight lunar feldspathic and mare basalts, and for three terrestrial and one lunar plutonic rock (Tables 3 and 4). The various distribution coefficients are listed in Table 5.

Basaltic Samples

Figure 1a shows a close approach to $K_{P-L}^{Mg} \sim .04$ for both lunar and terrestrial basaltic samples. Recorded MgO ranges up to 0.75 mole %. The high-Ti lunar basalts show the great deviations. However, Figure 1b shows that terrestrial plagioclase has significantly higher iron concentration than lunar plagioclase at a given concentration of iron in the liquid. Given the similar values of terrestrial and lunar K_{P-L}^{Mg} , the major cause of the higher Fe concentrations in terrestrial plagioclase is not likely to be an effect of the lower

$\frac{Ca}{Ca + Na + K}$ ratios of the terrestrial plagioclase, but rather the presence of ferric iron in terrestrial plagioclase-liquid pairs.

For K_{P-L}^{Fe} (where "Fe" = $Fe^{+2} + Fe^{+3}$) to be greater than K_{P-L}^{Fe} , $(Fe^{+3}/Fe^{+2})_P$ must exceed $(Fe^{+3}/Fe^{+2})_L$. Assuming that values of $K_{P-L}^{Fe^{+2}}$ are similar for lunar and terrestrial crystal-liquid pairs as are the values for K_{P-L}^{Mg} , between two-thirds and three-fourths of the iron in the terrestrial plagioclase is ferric.

Figure 2 shows the exchange relations of Fe and Mg for the natural plagioclase-liquid pairs. The value of K_{P-L}^{Fe-Mg} (~ 0.5) for the lunar low-Ti basalts means that at low oxygen fugacity X_P^{Fe} will be considerably lower than X_L^{Fe} . K_{P-L}^{Fe-Mg} increases with increasing oxygen fugacity and has an average

value of 1.4 for terrestrial basalts, so $X_P^{Fe^*} > X_L^{Fe^*}$. Presumably, if we could correct for all the ferric iron in the analyses of the terrestrial plagioclase and glasses we would observe an average value of K_{P-L}^{Fe-Mg} close to 0.5. The variation of $K_{P-L}^{Fe^*-Mg}$ with oxygen fugacity provides a crude oxygen barometer: in environments more oxidizing than those of terrestrial basalts, $K_{P-L}^{Fe^*-Mg}$ would have values higher than 1.4.

Synthetic Plagioclase-Liquid Pairs

Figure 3a shows the simple Mg distribution between synthetic plagioclase and coexisting liquid. Even though the temperatures of equilibration spanned a limited range (1218°C-1189°C) as opposed to the range of 1425°C to 1050°C for the natural samples, there is a good deal less coherence to the distribution between synthetic crystal-liquid pairs: the relative error ($\pm 1\sigma/\bar{K}_{P-L}$) for the terrestrial K_{P-L}^{Mg} is $\pm 22\%$, whereas for the synthetic pairs it is $\pm 30\%$. In Figure 3b we have plotted the MgO concentration in plagioclase versus the Temkin activity product $[CaO]_L^* [MgO]_L^* ([SiO_2]_L^*)^3$. The relative error of the average $K_{P-L}^{Mg^*}$ is now $\pm 15\%$. Thus much of the variability of K_{P-L}^{Mg} in Figure 3a is due to compositional effects. The plagioclase-liquid distribution of Fe shows a similar compositional dependence although the reduction of the relative error is not as great: $K_{P-L}^{Fe} = 0.033 \pm 0.010$ ($\pm 30\%$), whereas $K_{P-L}^{Fe^*} = 0.072 \pm 0.017$ ($\pm 24\%$). Errors from inaccurate application of the Fe secondary fluorescence correction at

inclined plagioclase-glass boundaries may cause higher relative errors in $K_{P-L}^{Fe^*}$ than $K_{P-L}^{Mg^*}$.

Besides lack of complete equilibration and multi-site substitution, another factor which may affect the inferred magnitude of the single element distribution coefficients is the diffusion controlled buildup of rejected elements marginal to growing crystals (Albarede and Bottinga, 1972). Because the plagioclase-liquid distribution coefficients of Fe and Mg are much less than one, they are particularly susceptible to errors induced by the under-estimation of FeO and MgO contents in the liquid. Longhi (1976) reported negligible enrichments of MgO marginal to plagioclase from Makaopuhi lava lake, so relatively slowly cooled natural plagioclase apparently does not yield erroneously high distribution coefficients. However, Kirkpatrick *et al.* (1976) report more than two orders of magnitude difference in the growth rate of anorthite at 5° to 20°C undercooling. Thus it is reasonable to expect some variability in the magnitudes of the single element distribution coefficients among synthetic crystal-liquid pairs grown at different undercoolings, and since these undercoolings are probably larger than those of the more slowly cooled natural liquids we can expect synthetic, single element distribution coefficients to be somewhat larger than those determined from the more slowly cooled natural samples (Table 5). Since, however, K_{P-L}^{Mg} and K_{P-L}^{Fe} have similar magnitudes, there will be little kinetic fractionation of Fe and Mg, and thus natural and synthetic values of K_{P-L}^{Fe-Mg} ought to be similar (Table 5).

Figure 4 shows the Fe-Mg exchange relations for the synthetic plagioclase-liquid pairs. Much of the spread in data points is probably due to errors in applying the correction for Fe secondary fluorescence. The relative counting errors do not exceed $\pm 10\%$ of $(\frac{Fe}{Fe + Mg})_P$. The average value of K_{P-L}^{Fe-Mg} of the natural low-Ti basalts (.49) is well within the error range of the synthetic K_{P-L}^{Fe-Mg} (.51 \pm .13). However, the average K_{P-L}^{Fe-Mg} for high-Ti basalts of .33 is significantly lower. Longhi *et al.* (1975) noted a similar effect of Ti upon K_{Ol-L}^{Fe-Mg} . Also shown in Figure 4 is the curve of constant $K_{Ol-L}^{Fe-Mg} = .33$ determined by Longhi *et al.* (1975) for lunar basaltic liquids. We see by comparison that at low oxygen fugacity and low total pressure the iron to magnesium ratio of plagioclase will be lower than that of coexisting low-Ti liquid but higher than that of coexisting olivine and probably orthopyroxene. Plagioclase coexisting with a high-Ti liquid will have X^{Fe} similar to coexisting olivine and orthopyroxene.

The absence of any large, systematic deviations of the data points in Figure 4 from the average value of K_{P-L}^{Fe-Mg} indicates that effects due to the two-site substitution of Fe and Mg are small in the range of $(\frac{Fe}{Fe + Mg})_L$ from .2 to .7.

Plutonic Samples

The limited analysis of plutonic plagioclase-liquid pairs is based upon three terrestrial samples (two from the Skaergaard intrusion--lower zone, one from the Ardnamurchan eucrite) and

one lunar--pink spinel troctolite (Prinz *et al.*, 1973). Liquid concentrations of FeO and MgO are calculated from the compositions of coexisting olivines by the equations of Roeder and Emslie (1972) and Longhi *et al.* (1975) by estimating temperatures of equilibration. For the terrestrial liquids FeO is converted to "FeO" (= FeO + FeO_{1.5}) by assuming $(\frac{Fe^{+3}}{Fe^{+2}})_L = 0.2$ (Longhi, 1976). Plutonic plagioclase-liquid pairs have considerably lower values of single element distribution coefficients, but higher values of K_{P-L}^{Fe-Mg} than do their low pressure counterparts (Table 5). The first observation is the result of lower concentrations of FeO and MgO in plutonic plagioclase than in basaltic plagioclase. As noted above, the absence of significant MgO gradients in the melt marginal to lava lake plagioclase precludes a kinetic/diffusion explanation for the difference in K_{P-L}^{Fe} and K_{P-L}^{Mg} between lava-lake basalts and plutonic rocks. In order for the differences in distribution coefficients to be due entirely to a pressure effect, the partial molar volumes of CaFeSi₃O₈ and CaMgSi₃O₈ must not only be considerably larger than that of anorthite, but also be approximately equal to one another. The latter is doubtful.

An alternative explanation of the differences in distribution coefficients lies in the dependence of the distribution coefficients upon liquid undercooling (or supersaturation). Hopper and Uhlmann (1974) show that the kinetic crystal-liquid distribution coefficient for a growing crystal is a function of undercooling, and that for isothermal growth

the compositions of crystal and liquid are closer together than the equilibrium compositions. Lofgren (1973) has demonstrated this effect for plagioclase. The smaller the undercooling, the closer the approach to the equilibrium compositions. Thus plagioclase growing under conditions of slow cooling and hence relatively small undercooling is able to exclude iron and magnesium more effectively. More rapidly cooled basaltic plagioclase shows the kinetic effects of larger undercooling with a consequently enhanced incorporation of iron and magnesium.

Whether this kinetic effect or the pressure effect can adequately explain the differences in observed distribution coefficients among plutonic and volcanic rocks is not known. It seems best, however, to treat distribution coefficients from these two types of rocks separately at this time.

Thermal Dependence of the Distribution Coefficients

The similarity of values of K_{P-L}^{Mg} for natural plagioclase-liquid pairs that span a range of temperature of more than 300°C is an indication that the temperature dependence is small. The temperatures of the submarine basalt liquids have been calculated from olivine-liquid equilibria by Frey *et al.* (1974); the temperatures of the lava lake samples are obtained by direct measurement and are listed by Kirkpatrick (1976). Log K_{P-L}^{Mg} and log K_{P-L}^{Mg*} for the terrestrial basaltic samples are assumed to be linear functions of $1/T^{\circ}K$. Regression equations in the form $\log K = A/T^{\circ}K + B$ are listed in Table 6 along with similar equations for olivine determined by Longhi *et al.* (1975). The olivine-liquid distribution coefficients, K_{Ol-L}^{Fe} and K_{Ol-L}^{Mg} , show similar temperature dependences; it is likely that the temperature dependencies of K_{P-L}^{Fe} and K_{P-L}^{Fe*} will be similar to K_{P-L}^{Mg} and K_{P-L}^{Mg*} respectively. The plagioclase-liquid pairs have smaller values of A indicating a weaker thermal dependence than the olivine equilibria; also the linear plots are relatively poor fits to the plagioclase data. Therefore, neither log K_{P-L}^{Mg} nor log K_{P-L}^{Mg*} is a useful geothermometer; on the contrary, single values of the plagioclase-liquid distribution coefficients may be employed throughout the crystallization interval with little thermal error. We can expect the temperature dependence of K_{P-L}^{Fe-Mg} to be even smaller than that of K_{P-L}^{Mg} .

Applications

Since Fe and Mg substitute in a systematic, predictable manner in plagioclase we may employ the concentrations of these elements in plagioclase to calculate liquid compositions and as a crystallization index. A crude, but potentially useful application to oxygen barometry has been noted above. And now that distribution coefficients are known it may become possible to calculate from the models of Smith et al. (1955) and Hopper and Uhlmann (1974) the crystal growth rate of plagioclase in quenched melts by measuring the diffusion controlled gradient of MgO in the melt marginal to plagioclase. There are three simple applications to lunar petrology.

Anorthosites

The presence of plagioclase in the anorthosites with relatively high anorthite contents (An_{96-98}) coupled with pyroxenes of intermediate X^{Fe} (0.3-0.6) poses a thorny interpretive problem. Smith and Steele (1974), noting that much of the pyroxene in these rocks in the form of rods and stringers a few microns wide appears to be exsolved from the plagioclase, suggested that X^{Fe} of these pyroxene crystals represented the original X^{Fe} of the plagioclase and that, therefore, the X^{Fe} of the liquid from which the anorthosites crystallized could be calculated from K_{P-L}^{Fe-Mg} . They obtained a value of $K_{P-L}^{Fe-Mg} = 2$ from three published plagioclase-liquid pairs and were thus able to calculate

values of X_L^{Fe} less than 0.2, which in turn led them to the conclusion that the anorthosites had crystallized from a relatively primitive liquid. In view of the distribution data presented above such an origin is unlikely.

Since no corrections for Fe secondary fluorescence were made in the original work, we are certain that the value of $K_{P-L}^{Fe-Mg} = 2$ is erroneously high. Given the measured values of $K_{P-L}^{Fe-Mg} < 1$ for lunar basaltic and plutonic rocks, we may conclude that if the small rods and stringers of pyroxene are in fact the result of the complete exsolution of Fe and Mg in plagioclase, then the anorthosites crystallized liquids with intermediate X^{Fe} .

The application of distribution data to anorthosites is by no means simple, however, because Walker et al. (1973) and Dixon and Papike (1975) have shown that plagioclase in the anorthosites (e.g., 60025) may retain measurable amounts of Fe and Mg in the presence of these small pyroxenes. If these small pyroxenes are exsolutions then neither the X^{Fe} of pyroxenes nor plagioclase may represent the original X_P^{Fe} . If the small pyroxenes are primary inclusions then some metamorphic exchange of Fe and Mg between plagioclase and pyroxene may have altered the original X^{Fe} of both pyroxene and plagioclase. Regardless of which of these possibilities is correct the original X_P^{Fe} in 60025 must be greater than or equal to the present $X_{Px}^{Fe} = 0.35 - 0.45$ and less than or equal to the present

$X_P^{Fe} > 0.5$ (Walker *et al.*, 1973). Application of a lunar K_{P-L}^{Fe-Mg} (0.5 - 0.7) then leads us to the conclusion that 60025 crystallized from a liquid with $Fe/(Fe + Mg) \approx 0.6 - 0.7$.

Zonation

There are many published reports of Fe and Mg zonation in basaltic plagioclase, however, some workers have been skeptical of the conclusions reached because the secondary fluorescence effect alone will produce an apparent Fe zonation. We, therefore, present several patterns of fluorescence-corrected plagioclase zonation to demonstrate the utility of X_P^{Fe} variation.

In Figure 5a, "anorthite" content ($\frac{Ca}{Ca + Na + K}$) is plotted as a function of X_P^{Fe} for plagioclase cores, mantles and rims in two slowly cooled mare basalts, 15555 and 15065, with plagioclase poikilitic texture. As X_P^{Fe} increases, anorthite content decreases much as expected. Zoning in most individual crystals follows the general pattern--cores have the highest $\frac{Ca}{Ca + Na + K}$, the lowest X^{Fe} , whereas the rims have the lowest $\frac{Ca}{Ca + Na + K}$ and highest X^{Fe} --an indication of outward growth. However, note that one of the crystals in 15065 has its highest $\frac{Ca}{Ca + Na + K}$ and lowest X^{Fe} at its rims. This apparent reversed zoning is consistent with nucleation of the plagioclase upon separate pyroxene crystals and subsequent growth inward into the volume between the pyroxene crystals.

In Figure 5b are similar plots of plagioclase zonation for

two-finer grained mare basalts, 12002 and 12021, in which plagioclase laths commonly have hollow cores: In contrast to Figure 5a there is a small, overall increase in anorthite content with increasing X^{Fe} in the plagioclase. Crawford (1973) has previously observed this phenomenon in 12021. This sort of reversed zoning is consistent with delayed nucleation of plagioclase, followed by plagioclase crystallization at progressively decreasing under-cooling at near isothermal conditions (Hopper and Uhlmann, 1974; Lofgren, 1973).

Impact Melts

Variation of iron and magnesium in plagioclase may help identify chemical heterogeneity in igneous rocks, a clue to an impact origin (Simonds, 1975). Figure 6 is a plot of $\frac{Ca}{Ca + Na + K}$ vs. $\frac{Fe}{Fe + Mg}$ for the cores of the larger, texturally primitive blocky crystals and laths in rock 14310, a feldspathic basalt. The variation of $\frac{Ca}{Ca + Na + K}$ at constant $\frac{Fe}{Fe + Mg}$ is nearly twice as great as that in the mare basalts (Figure 5). Further, there is a structure to the variations--cores with $\frac{Ca}{Ca + Na + K} < 0.9$ have concentrations of $K_2O > .10$ mole % (generally greater than .15 % with a maximum of .25 %); cores with $\frac{Ca}{Ca + Na + K} > 0.9$ have concentrations of $K_2O < .10$ mole % (generally less than .05 %). Such variation of $\frac{Ca}{Ca + Na + K}$, $\frac{Fe}{Fe + Mg}$ and K_2O is not observed in plagioclase cores in the mare basalts which are truly volcanic. Although this rock was completely or nearly completely molten at one time,

14310 crystallized from a melt that was inhomogeneous. Morgan *et al.* (1972) identified rock 14310 as a probably impact melt on the basis of high, non-lunar siderophile element abundances. Schonfeld and Meyer (1972) showed that the bulk chemistry of this rock can be explained largely as a mixture of KREEP and anorthositic components. It seems logical to conclude, therefore, that the plagioclase cores with low $\frac{\text{Ca}}{\text{Ca} + \text{Na} + \text{K}}$ and high-K are ghosts of KREEP materials incompletely homogenized during the melting process.

Acknowledgements

The authors wish to thank W. B. Bryan, T. L. Grove, R. J. Kirkpatrick, J. R. Smyth and P. W. Weiblen for providing the natural samples. We also wish to thank W. B. Bryan, J. V. Smith and D. F. Weill for helpful discussions. This work was supported by NASA Grant NGL 22-007-247 and the Committee on Experimental Geology and Geophysics at Harvard University.

REFERENCES

- Albarede F. and Bottinga Y. (1972) Kinetic disequilibrium in trace element partitioning between phenocrysts and host lava. Geochim. Cosmochim. Acta 36, 141-156.
- Appleman D.E., Nissen H.U., Stewart D.B., Clark J.R., Dowty E. and Huebner S.J. (1971) Studies of lunar plagioclase, tridymite and cristobalite. Proc. Lunar Sci. Conf. 2nd, p. 117-133.
- Biggar G.M., O'Hara M.J., Peckett A. and Humphries D.J. (1971) Lunar lavas and the achondrites: petrogenesis of protohypersthene basalts. Proc. Lunar Sci. Conf. 2nd, p. 617-643.
- Bottinga Y. and Weill D.F. (1972) The viscosity of magmatic silicate liquids: a model for calculation. Am. J. Sci. 272, 438-475.
- Compston W., Berry H., Vernon M.J., Chappell B.W. and Kaye M.J. (1971) Rubidium-strontium chronology and chemistry of lunar material from the Ocean of Storms. Proc. Lunar Sci. Conf. 2nd, p. 1471-1485.
- Crawford M.L. (1973) Crystallization of plagioclase in mare basalts. Proc. Lunar Sci. Conf. 4th, p. 705-717.
- Dixon J.R. and Papike J.J. (1975) Petrology of anorthosites from the Descartes region of the moon: Apollo 16. Proc. Lunar Sci. Conf. 6th, p. 263-291.
- Drake M.J. and Weill D.F. (1975) Partition of Sr, Ba, Ca, Y,

- Eu⁺² and Eu⁺³ and other REE elements between plagioclase feldspar and magmatic liquid: an experimental study. Geochim. Cosmochim. Acta **38**, 689-712.
- Frey F.A., Bryan W.B. and Thompson G. (1974) Atlantic Ocean floor: Geochemistry and petrology of basalts from legs 2 and 3 of the Deep Sea Drilling Project. J. Geophys. Res. **79**, 5507-5528.
- Grover J.E. and Orville P.M. (1969) The partitioning of cations between coexisting single- and multi-site phases with application to the assemblages orthopyroxene-clinopyroxene and orthopyroxene-olivine. Geochim. Cosmochim. Acta **33**, 205-226.
- Hafner S.S., Virgo D. and Warburton D. (1971) Oxidation state of iron in plagioclase from lunar basalts. Earth Planet. Sci. Lett. **12**, 159-166.
- Hopper R.W. and Uhlmann D.R. (1974) Solute redistribution during crystallization at constant velocity and constant temperature. J. Cryst. Growth **21**, 203-213.
- Kesson S.E. (1975) Mare basalt petrogenesis. Proc. Conf. Origins Mare Basalts, 81-84.
- Kirkpatrick R.J. (1976) Nucleation and growth of plagioclase in the Hawaiian lava lakes Makaopuhi and Alae. Bull. Geol. Soc. Am. Submitted.
- Kirkpatrick R.J., Robinson G.R. and Hays J.F. (1976) Kinetics of crystal growth for silicate melts: anorthite and

- diopside. J. Geophys. Res. Submitted.
- Lofgren G. (1973) Temperature induced zoning in synthetic plagioclase feldspar. In Proceedings of NATO Conference on Feldspars. W.S. McKenzie and J. Zussman, Eds.
- Longhi J. (1976) Iron, magnesium and silica in plagioclase. Unpublished Ph.D. thesis, Harvard University.
- Longhi J., Walker D., Grove T.L., Stolper E.N. and Hays J.F. (1974) The petrology of the Apollo 17 mare basalts. Proc. Lunar Sci. Conf. **5th**, p. 447-469.
- Longhi J., Walker D. and Hays J.F. (1976) Fe, Mg and silica in lunar plagioclase (abstract). In Lunar Science VII, p. 501-503. The Lunar Science Institute, Houston.
- Longhi J., Walker D. and Hays J.F. (1975) The distribution of Fe and Mg between olivine and lunar basaltic melts (abstract). EOS **56**, 471.
- Longhi J., Walker D. and Hays J.F. (1972) Petrography and crystallization history of basalts 14310 and 14072. Proc. Lunar Sci. Conf. **3rd**, p. 131-139.
- LSPET (1971) Preliminary examination of lunar samples from Apollo 14. Science **173**, 681-683.
- Morgan J.W., Laul J.C., Kröhenbuhl U., Ganapathy R. and Anders E. (1972) Major impacts on the moon: characterization from trace elements in Apollo 12 and 14 samples. Proc. Lunar Sci. Conf. **3rd**, p. 1377-1395.
- Prinz M., Dowty E., Keil K. and Bunch T.E. (1973) Spinel troctolite and anorthosite in Apollo 16 samples. Science **179**, 74-76.
- Roeder P.L. and Emslie R.F. (1970) Olivine-liquid equilibrium.

- Contr. Mineral. and Petrol. 29, 275-289.
- Schonfeld E. and Meyer C. Jr. (1972) The abundances of components of the lunar soils by a least squares mixing model and the formation age of KREEP. Proc. Lunar Sci. Conf. 3rd, p. 1397-1420.
- Simonds C.H. (1975) Thermal regimes in impact melts and the petrology of the Apollo 17 Station 6 boulder. Proc. Lunar Sci. Conf. 6th, p. 641-672.
- Smith J.V. (1965) X-ray emission micro-analysis of rock-forming minerals. I. Experimental techniques. J. Geol. 73, 830-864.
- Smith J.V. and Steele I.M. (1974) Intergrowths in lunar and terrestrial anorthosites with implications for lunar differentiation. Amer. Mineral. 59, 673-680.
- Smith V.G., Tiller W.A. and Rutter J.W. (1955) A mathematical analysis of solute redistribution during solidification. Can. J. Phys. 33, 723-745.
- Temkin M. (1945) Mixtures of fused salts as ionic solutions. Acta Physicochemica, U.S.S.R. 20, 411-420.
- Walker D., Kirkpatrick R.J., Longhi J. and Hays J.F. (1976) Crystallization history of lunar picrite basalt sample 12002: Phase equilibria and cooling rate studies. Bull. Geol. Soc. Am. In Press.
- Walker D., Longhi J., Stolper E.N., Grove T.L. and Hays J.F. (1975) Origin of titaniferous lunar basalts. Geochim.

- Cosmochim. Acta 39, 1219-1235.
- Walker D., Longhi J., Grove T.L., Stolper E.N. and Hays J.F. (1973) Experimental petrology and origin of rocks from the Descartes Highlands. Proc. Lunar Sci. Conf. 4th, p. 1013-1032.
- Walker D., Longhi J. and Hays J.F. (1972) Experimental petrology and origin of Frau Mauro rocks and soil. Proc. Lunar Sci. Conf. 3rd, p. 797-817.
- Weill D.F., McCallum I.S., Bottinga Y., Drake M.J. and McKay G.A. (1970) Mineralogy and petrology of some Apollo 11 igneous rocks. Proc. Apollo 11 Lunar Sci. Conf., p. 937-956.
- Wenk H.R. and Wilde W.R. (1973) Chemical anomalies of lunar plagioclase, described by substitution vectors and their relation to optical and structural properties. Contr. Mineral. and Petrol. 41, 89-104.

Table 1. Plagioclase - liquid distribution data: Terrestrial basalts

	Submarine				Hakapouhi Lava Lake			
	WT5-L 3-14-10-1	3-15-10-1	3-18-17-1	2-10-19-1	MP68-1-21	MP68-2-20	MP10-14	MP 22-13
SiO ₂	48.28	49.90	48.74	48.41	50.97	52.23	51.90	57.34
TiO ₂	.86	2.23	.80	1.53	4.51	4.22	4.67	2.46
Al ₂ O ₃	16.62	13.35	16.44	9.69	12.08	12.04	11.92	12.21
Cr ₂ O ₃	n.d.	n.d.	n.d.	n.d.	.01	n.d.	n.d.	n.d.
FeO*	8.17	11.45	7.95	8.73	13.21	14.72	14.54	12.51
MgO	9.56	6.41	9.88	7.50	4.67	3.56	3.54	1.87
CaO	12.61	10.89	12.76	11.80	8.73	7.81	7.90	5.57
K ₂ O	.01	.11	.02	.45	.88	1.23	1.28	2.53
Na ₂ O	2.11	2.90	1.77	2.52	2.66	2.56	2.44	2.39
Sum	98.22	97.25	98.35	96.70	97.73	98.37	98.18	96.87
atomic Fe/Fe+Mg	.324	.501	.311	.395	.613	.699	.697	.790
POC	121301	no olivine	122001	117401	108202	106002	106002	10472
wt% mole % (FeO) _p *	.45	.63	.38	.42	.68	.67	.67	.70
(MgO) _p	.58	.40	.56	.46	.26	.22	.27	.16
no. analyzed plag.	7	11	9	9	5	9	8	8

1. Frey et al. (1974)
2. Kirkpatrick (1976)

* All Fe as FeO

Figure Captions

Figure 1a. Simple molar MgO distribution between calcic plagioclase and natural basaltic liquids. Lunar liquid compositions are all estimated;

1b. Simple molar "FeO" distribution between calcic plagioclase and natural basaltic liquids, where "FeO" is total iron as FeO. Symbols same as in 1a.

Figure 2. Exchange relations of Fe and Mg between plagioclase and natural basaltic liquids. Symbols same as in Figure 1.

Figure 3a. Simple molar MgO distribution between synthetic plagioclase-liquid pairs. Temperature range is 1189° to 1218°C. P = pyroxene present.

3b. MgO concentration in synthetic plagioclase as a function of Temkin model activity product;

Figure 4. Exchange relations of Fe and Mg between synthetic plagioclase and liquid. K_{Ol-L}^{Fe-Mg} from Longhi et al. (1975).

Figure 5a. Plagioclase zonation in coarse grained mare basalts, 15555 and 15065 with plagioclase poikilitic texture. C = core, R = rim.

5b. Plagioclase zonation in fine-grained mare basalts, 12002 and 12021, with hollow plagioclase laths.

Figure 6. Anorthite content versus $(Fe/Fe + Mg)_p$ in plagioclase cores from lunar feldspathic basalt, 14310. High K # mole % $K_2O > .10$.

Table 2. Plagioclase-liquid distribution data

Synthetic Alkali-Free Compositions; Fe Capsules

	RFC.2-18	RFC.3-18	TFC.4-12	TFC.4-4	QFC.5-17	DFC.6-13
wt% SiO ₂	54.18	54.77	57.76	56.15	52.78	51.85
TiO ₂	.90	.87	1.07	1.11	n.d.	1.16
Al ₂ O ₃	15.59	14.81	16.13	15.05	13.77	15.19
Cr ₂ O ₃	0.00	.11	.14	n.d.	n.d.	.22
FeO	7.68	7.68	4.87	6.19	8.12	12.74
MgO	8.32	7.94	9.24	8.58	6.73	5.89
CaO	11.75	12.27	11.98	11.75	15.66	12.65
K ₂ O	0.00	0.00	.01	n.d.	n.d.	.01
Na ₂ O	0.00	.07	0.00	n.d.	n.d.	0.00
Sum	98.42	98.53	101.19	98.82	97.06	99.71
atomic $\frac{Fe}{Fe + Mg}$.340	.352	.220	.288	.404	.548
Temp (°C)	1224/1189	1224/1189	1257/1218	1241/1212	1233/1199	1257/1218
Time (hrs)	48/168	48/168	50/240	48/210	96/225	50/240
Other phases	opx?	opx	-	opx	-	-
avg. mole%						
(FeO) _p	.26	.26	.12	.24	.32	.36
(MgO) _p	1.06	1.03	.84	.85	1.00	.60
plag. analyzed	2	3	2	5	5	2

Table 2 (continued). Plagioclase-liquid distribution data

Synthetic Alkali-Free Compositions; Fe Capsules

	DFC.6-14	DFC.6-15	DFC.7-12	DFC.7-15	DFC.8-18
wt% SiO ₂	49.94	51.16	45.79	48.48	49.13
TiO ₂	1.25	1.25	1.06	1.12	1.18
Al ₂ O ₃	14.69	14.13	14.15	13.71	13.16
Cr ₂ O ₃	n.d.	n.d.	n.d.	n.d.	n.d.
FeO	12.17	12.35	19.20	16.31	16.05
MgO	6.29	6.50	5.79	6.27	5.47
CaO	12.59	12.45	11.69	11.99	12.30
K ₂ O	n.d.	n.d.	n.d.	n.d.	n.d.
Na ₂ O	n.d.	n.d.	n.d.	n.d.	n.d.
Sum	96.93	97.03	97.68	97.88	97.28
atomic $\frac{Fe}{Fe + Mg}$.520	.516	.650	.593	.622
Temp (°C)	1240/1217	1241/1212	1241/1212	1233/1206	1233/1206
Time (hrs)	40/211	40/210	48/210	48/168	48/168
Other phases	-	-	-	-	-
avg. mole%					
(FeO) _p	.39	.34	.44	.35	.31
(MgO) _p	.60	.66	.47	.53	.39
no. plag. analyzed	4	9	8	5	3

TABLE 3
PLAGIOCLASE-LIQUID DISTRIBUTION DATA: NATURAL LUNAR BASALTS

Wt%-L	feldspathic		low-Ti mare			high-Ti mare		
	68415 ¹	68415- (10% An ₉₈)*	14310 ²	15555 ³	15065 ³	12038 ⁴	70017 ⁵	75035 ⁶
SiO ₂	45.3	45.7	48.27	45.8	46.1	46.56	41.1	41.6
TiO ₂	.35	.39	1.27	3.26	2.53	3.31	10.3	10.2
Al ₂ O ₃	28.7	28.0	20.26	10.8	11.1	12.53	9.99	9.75
Cr ₂ O ₃	.14	.16	.20	.29	.31	.27	.31	.27
FeO	3.69	4.12	8.11	20.0	20.1	17.99	19.0	18.5
MgO	4.44	4.96	7.76	5.74	5.55	6.71	6.44	6.16
MnO	-	-	-	.31	.32	.27	-	.30
CaO	16.3	16.0	12.25	11.7	11.4	11.62	11.3	11.5
K ₂ O	.12	.13	.81	-	-	.07	.05	-
Na ₂ O	.5	.54	.55	.14	.17	.66	.20	.48
Sum	100.4	100.0	99.48	98.0	97.7	99.99	98.7	98.8
atomic Fe/Fe + Mg	.31	.31	.34	.66	.67	.59	.62	.63
T°C	~1425 ^o	<1400 ^o C	~1325 ^o	1150 ^o	1147 ^o	1160 ^o 7	1144 ^o	1137 ^o
avg. mole %								
FeO _p	.04	.08	.16	.40	.35	.25	.32	.34
MgO _p	.20	.35	.48	.38	.30	.50	.68	.54

*Sample may contain unmelted or xenocrystal material--An₉₈

- | | |
|----------------------------------|--------------------------------|
| 1. Walker <u>et al.</u> (1973) | 5. Longhi <u>et al.</u> (1974) |
| 2. Walker <u>et al.</u> (1972) | 6. Walker <u>et al.</u> (1975) |
| 3. unpublished experimental data | 7. Biggar <u>et al.</u> (1971) |
| 4. Compston <u>et al.</u> (1971) | |

TABLE 4
PLAGIOCLASE-LIQUID DISTRIBUTION DATA: PLUTONIC ROCKS

Mole %	lunar		terrestrial		
	Pink-spinel troctolite ¹		Skaergaard LZA	Skaergaard LZ-MBG	Ardnamurchan euclite
	67435	65785			
FeO _L	5.0	10.8	24.7	17.2	19.6
MgO _L	60.9	55.8	41.9	48.7	46.6
FeO _L ²	5.0	10.8	17.3	12.0	13.7
MgO _L ²	20.0	18.4	8.91	10.4	9.99
"FeO" _L	-	-	20.8	14.4	16.4
T°C	1270 ^o 3		1200 ^o 4	1200 ^o 4	1200 ^o 4
"FeO" _p	.05		.33	.29	.63
MgO _p	.17		.06	.04	.08

1. Olivine preceded plagioclase in 67435, but crystallized after plagioclase in 65785, hence the actual FeO_L and MgO_L are taken to be the average of the computed values.
2. Calculations based upon equations of Roeder and Emslie (1970) and Longhi et al. (1975)-- see table 6 of this study.
3. Walker et al. (1973).
4. Estimated.

TABLE 5
DISTRIBUTION COEFFICIENTS

	Mole Fraction				
	K_{P-L}^{Fe}	K_{P-L}^{Mg}	$K_{P-L}^{Fe^*}$	$K_{P-L}^{Mg^*}$	K_{P-L}^{Fe-Mg}
Lunar					
Basaltic					
low-Ti	.020	.041	.056	.12	.49
high-Ti	.020	.061	.075	.24	.33
Plutonic					
(P.S.T.)	.006	.009	.03	.04	.7
Terrestrial					
Basaltic	.058	.041	.18	.13	1.4
	$\pm .008$	$\pm .009$	$\pm .02$	$\pm .03$	$\pm .3$
Plutonic	.025	.0063			4.2
Synthetic	.033	.065	.072	.14	.51
	$\pm .010$	$\pm .016$	$\pm .017$	$\pm .02$	$\pm .13$

TABLE 6
TEMPERATURE DEPENDENCE OF DISTRIBUTION COEFFICIENTS

$$\log K = \frac{A}{TOK} + B; r = \text{correlation coefficient}$$

K	A	B	r
K_{P-L}^{Mg}	1216	2.265	.48
$K_{P-L}^{Mg^*}$	1255	1.787	.50
$K_{O1-L}^{Fe^*}$	2818	1.212	.97
$K_{O1-L}^{Mg^*}$	2616	1.825	.95

¹Longhi et al. (1975)--low-Ti olivine-liquid pairs.

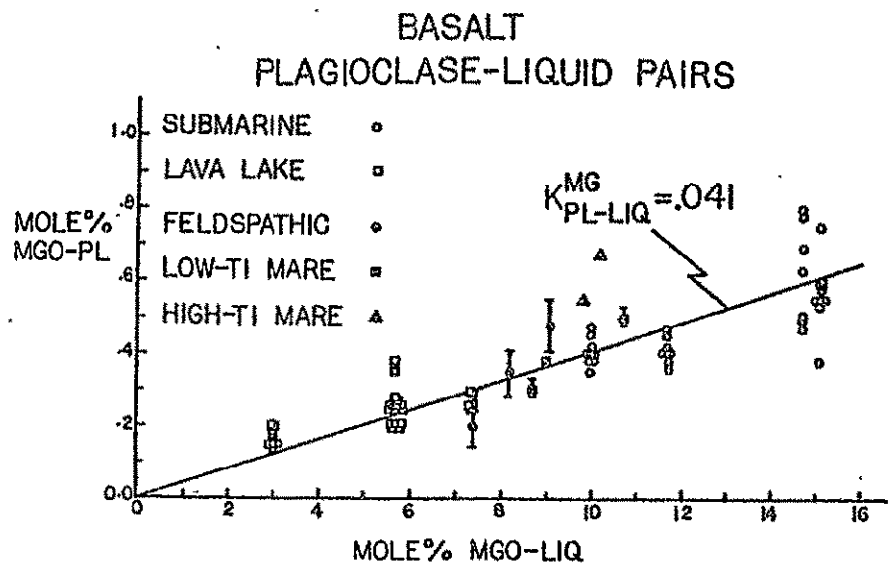


Fig. 1a Longhi et al.
Fe+Mg Plaq 5/28/76

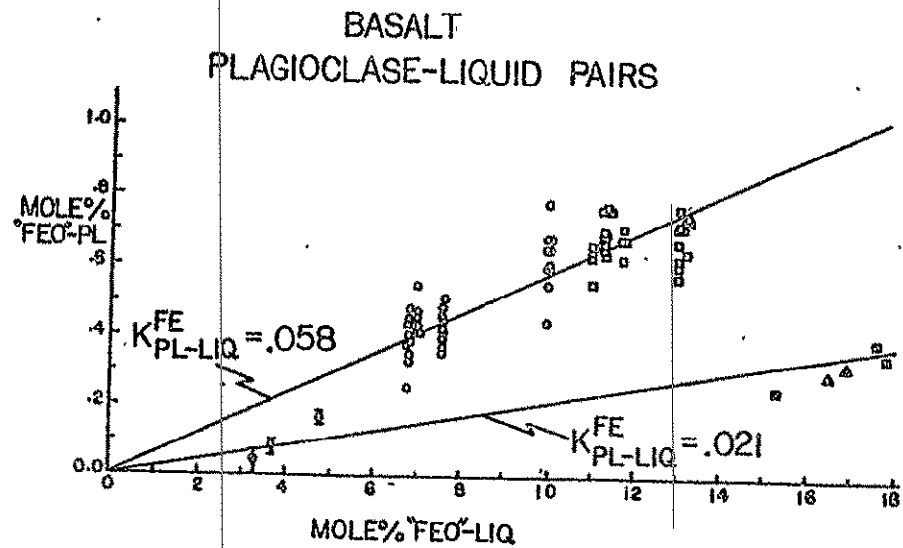


Fig. 1b Longhi et al.
Fe+Mg Plaq 5/28/76

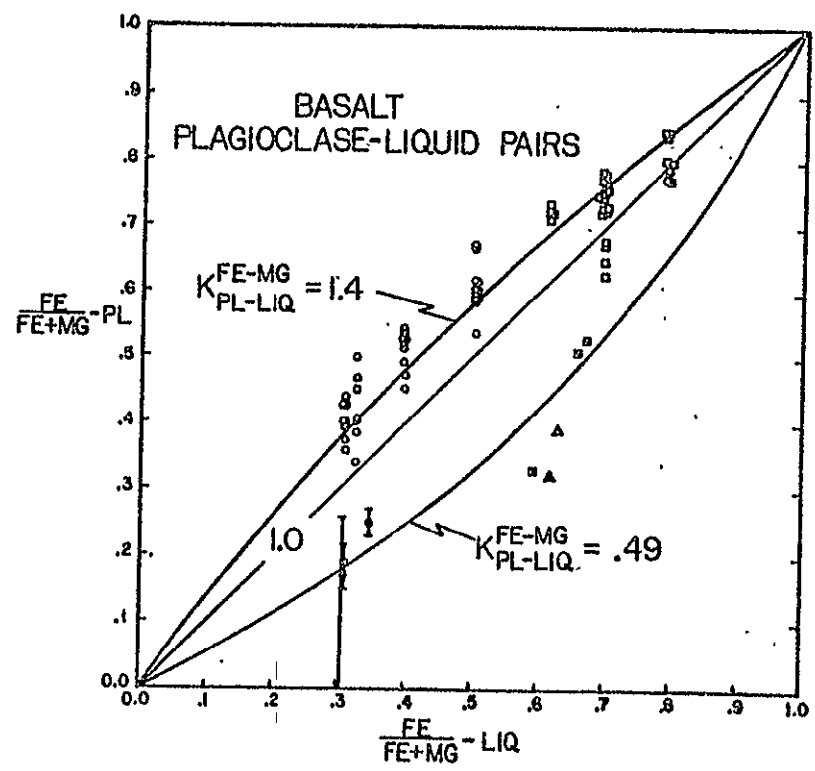


Fig. 2 Longhi et al.
F.L.M. Pl. 5/14/77

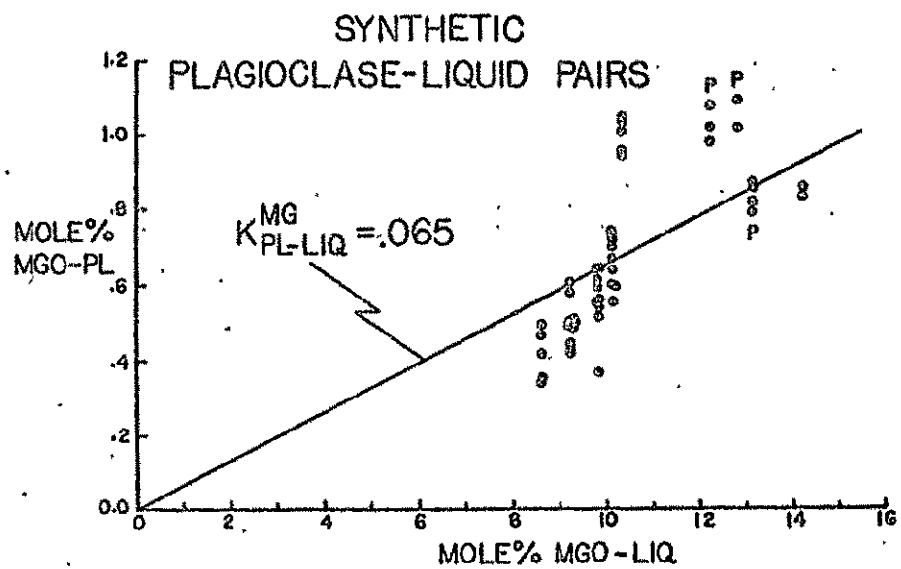


Fig. 3a Longhi et al.
Form Plac. 5/28/76

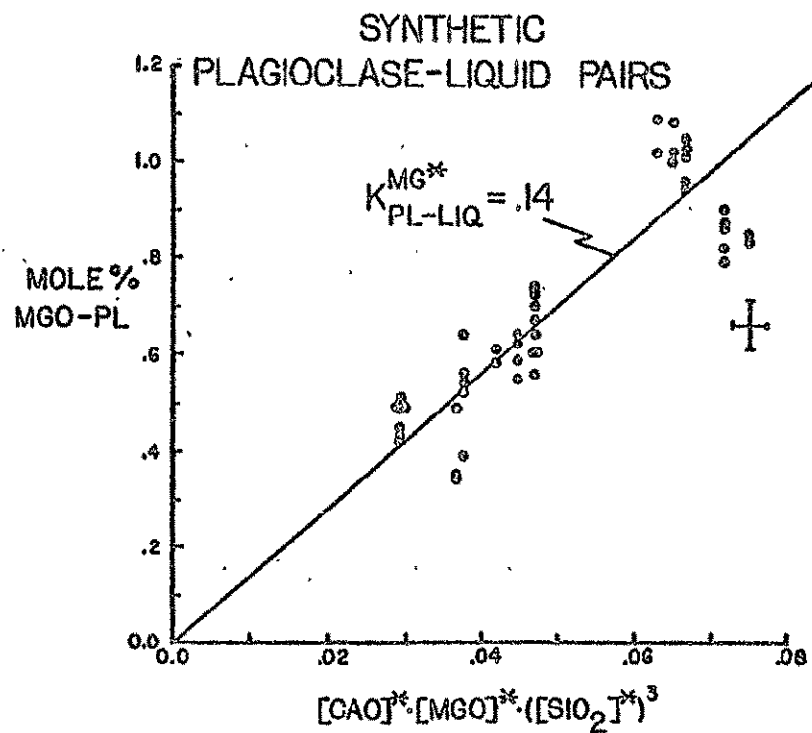


Fig. 3b Longhi et al.
Form Plac. 5/28/76

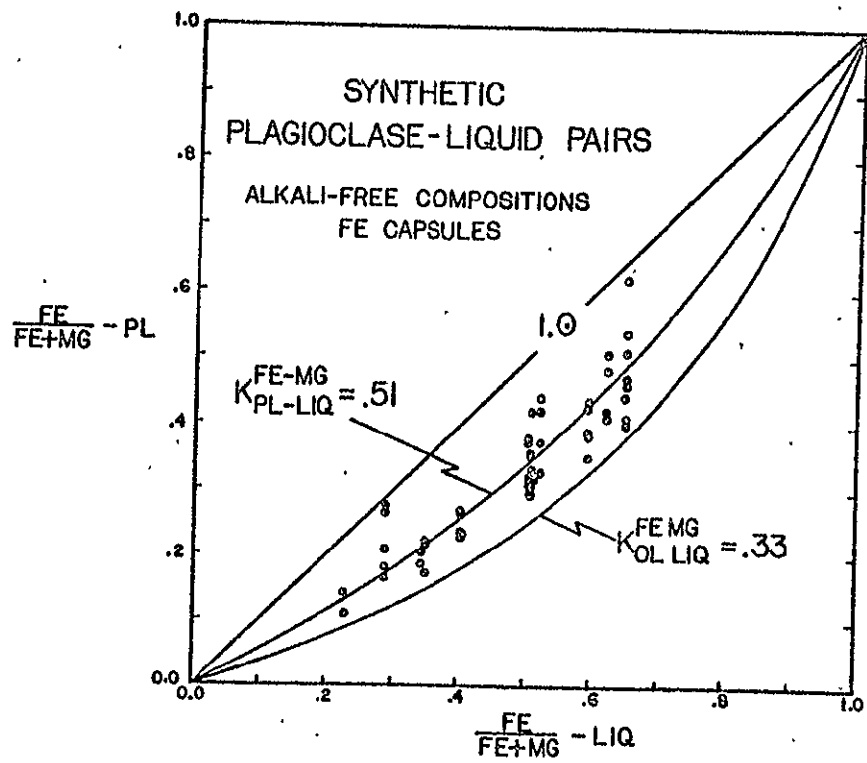


Fig 4 Longhi et al.
Fe+Mg Plas 5/28/76

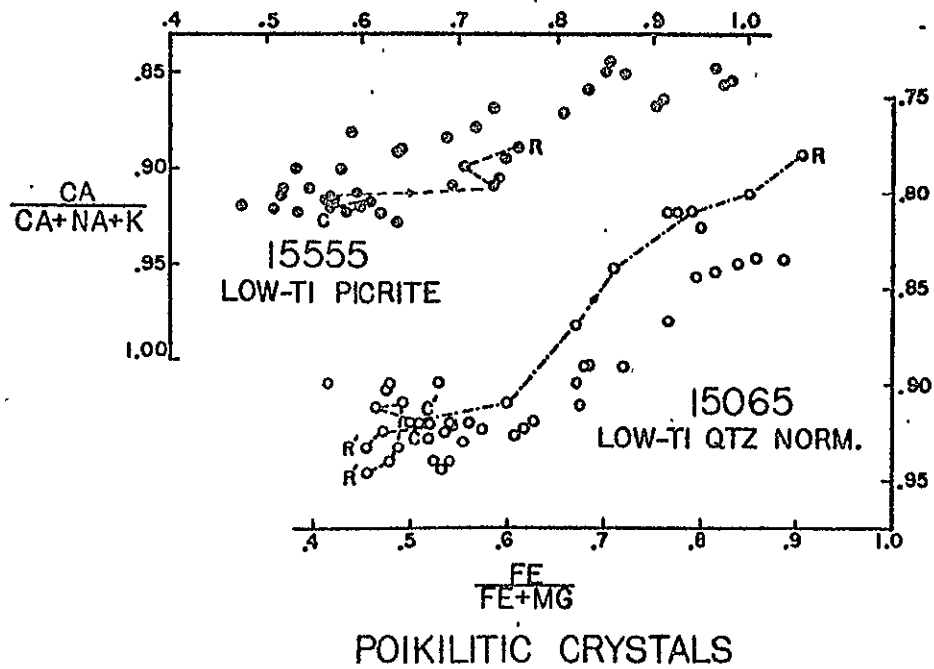


Fig. 5 a
Fe+Mg Plaq.

Longhi et al.
5/28/76

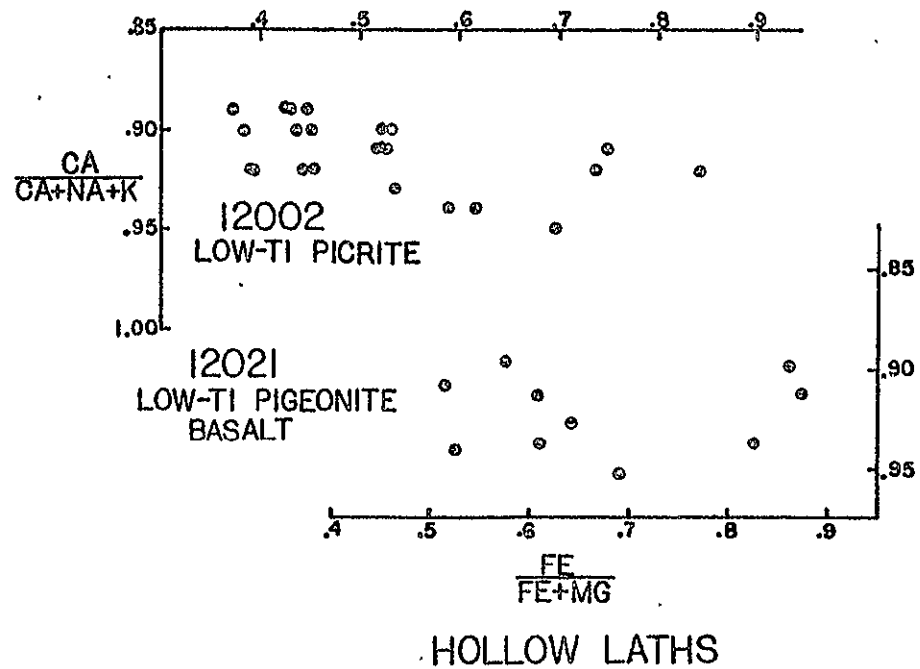


Fig. 5 b
Fe+Mg Plaq.

Longhi et al.
5/28/76

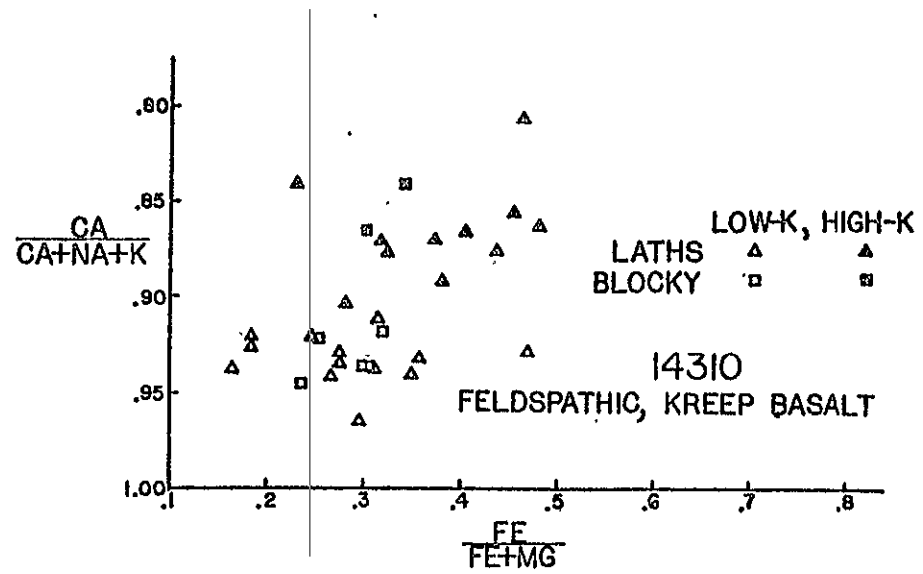


Fig 6
F.M. Plas

Longhi et al.
5/28/76

DIFFERENTIATION OF AN APOLLO 12 PICRITE MAGMA

David Walker,¹ John Longhi,² R. James Kirkpatrick,³
and James F. Hays¹

Revised Version: May 28, 1976

¹Hoffman Laboratory, Harvard University
Cambridge, Mass. 02138

²Dept. Earth and Planetary Sciences, Massachusetts Institute
of Technology, Cambridge, Mass. 02139

³Deep Sea Drilling Project, A031
University of California, San Diego,
La Jolla, California 92093

Submitted to Proceedings of 7th Lunar Science Conference

ABSTRACT

The Apollo 12 olivine basalt suite shows a strong positive correlation of grain size with normative olivine content. This correlation is interpreted to mean that the suite of samples represents the basal portion of a cooling unit which differentiated by simple olivine settling. The grain size of plagioclase observed in the coarsest samples indicates the cooling unit may have been as much as 30 meters thick. The amount of olivine concentration observed in the suite is quantitatively internally consistent with simple olivine settling in a magma body of this size which has the composition of the chill margin.

INTRODUCTION

The Apollo 12 olivine basalts form a coherent group whose major element chemistry can be related by olivine fractionation. Sufficient petrography and experimental petrology information exists to make a detailed analysis of the differentiation process of the magma body (or bodies) in which this suite of samples formed. This analysis is based on a simple model of gravitative olivine settling. Quantitative input for the model calculations comes from crystallization experiments at controlled cooling rates on one of the members of the suite. These experiments quantify the cooling history and the physical properties of the magma during solidification. It is the purpose of this paper to show the relation between the cooling

history, differentiation, and petrographic features of this suite of olivine basalts. Normative olivine abundance is the principle index of differentiation and grain size is the principle feature related to cooling history in our discussion, so our task is to explain the strong positive correlation between olivine abundance and grain size which is observed in this suite.

CHEMISTRY AND PETROGRAPHY

A sub-group of the Apollo 12 samples--the olivine basalts, picrites, and gabbros--has a major-element chemical variation which can be described to a good approximation by an addition or subtraction of olivine of about Fo_{74} (Kushiro and Haramura 1971; Compston et al., 1971; James and Wright, 1972). Green et al. (1971) showed that the liquidus olivine of the least olivine-normative member of the group (i.e., 12009) was of about this composition whereas the liquidus olivine of the more olivine-normative members was significantly more magnesian than any olivines actually observed in the suite. This led to the conclusion that the less olivine-normative members of the suite represented liquid magma compositions into which liquidus olivine accumulated to form the rest of the suite--a conclusion compatible with the observation that 12009 (the proposed magma composition) had a vitrophyric texture indicating quenching from a melt. Grove et al. (1973) and Walker et al. (1975) also supported this conclusion from work on 12002, a picrite near in composition to 12009.

Table 1 lists the normative olivine abundance for rocks in this suite taken from published chemical analyses. Normative olivine varies by more than a factor of two. Modal data collected on 1 to 3 sections of each rock are also listed. The correspondence of modal and normative olivine is acceptable for samples 12009, 12075, 12002, 12040, and 12035 but is quite poor for 12004, 12020, and 12018 which show too little modal olivine relative to the norm. Misidentification of pyroxene for olivine is not thought to be the cause of the discrepancy because James and Wright (1972, Table 13) also record this discrepancy for 12018 but not for 12020. This suggests that there may be significant heterogeneities in the distribution of the olivine phenocrysts in these samples. This is also suggested by the large range in the chemical mode for 12004 in Table 2A of James and Wright.

Figure 1 shows a series of photomicrographs of textures of rocks in this suite. The photos are arranged in order of increasing plagioclase grain size and a very obvious relation to normative olivine content is apparent. The coarser samples are more olivine-normative. Sample coarseness is determined by the grain size of the groundmass minerals. Although the olivine phenocrysts show a very limited range of size, there is a systematic variation in their habit. In 12009, the vitrophyre, the olivine phenocrysts are euhedral to euhedral-skeletal. As the samples coarsen the olivines become subhedral and lose all distinction as phenocrysts in the coarse-grained, holocrystalline gabbros. Pyroxene phenocrysts become equally indistinct in the coarse-grained gabbros and they are also absent in the vitrophyre.

Since pyroxenes are present both as phenocryst and groundmass minerals and therefore show quite a variety of morphologies and sizes in a single sample, groundmass plagioclase is preferred as an index of sample coarseness. Table 1 lists the average width of the largest plagioclase laths observed in thin section. The size varies by almost three orders of magnitude and it can be seen that there is an excellent correlation of plagioclase size with normative olivine content. This is shown graphically in Figure 2. Plagioclase size is a useful parameter of coarseness since it is more easily quantified than pyroxene size. [Furthermore, groundmass minerals grown after magma emplacement, such as plagioclase, are not as likely (as intratelluric phenocrysts are) to be distributed according to size during magma flow; and hence they are probably a better index of cooling history after emplacement.] The two minerals give generally similar ordering of coarseness by "eyeball" as can be seen from the study by Hodges and Papike (1975) who did not use plagioclase size specifically. Their coarseness ordering of 5 samples reversed only the adjacent pair 12075-12004 relative to the present sequence of 8 samples.

The fact that the chemistry of the samples can be related by olivine addition is assumed to mean that the samples are genetically related in this way. The specific composition of the magma will be taken up below. The attempt to reconstruct this suite of samples within a single magma body runs counter to some current thinking about lunar petrogenesis. Previous petrographic studies by James and Wright (1972) and Warner (1971) have tended

to separate the coarser and finer grained samples with the implication that they have a separate genesis. An exception to this approach is the study by Hodges and Papike (1975). It is perhaps the evidence from minor elements which in the past has most strongly suggested that any simple story implied by the correlation of petrography and major element chemistry is misleading. For example, Compston *et al.* (1971) showed that olivine fractionation alone cannot relate all the samples since at least three different subgroups of the suite can be recognized on the basis of Rb/Sr and initial $^{87}\text{Sr}/^{86}\text{Sr}$. Furthermore, R. A. Schmitt (personal communication) has pointed out that at least three subgroups, which cannot be related by simple olivine fractionation, are recognizable on the basis of La/Sm ratio. These groupings are not the same as the Rb/Sr ones. It would appear that these arguments are very powerful and that it may be necessary to abandon the notion that the whole suite is part of the same cooling unit. However, it should be noted that substantial isotopic inhomogeneity has been reported in Sr in a single recent terrestrial basalt flow (Laughlin *et al.*, 1972) which is presumably related to cryptic contamination. If such processes supplement olivine fractionation as a control on minor-element and isotopic chemistry in the lunar case, then it may not be necessary to abandon the idea that the samples are consanguinous. It is worth noting that even if the samples are not consanguinous, the process we shall explore here would have to occur in each of however many magma bodies of the same major-element composition are required by the minor-element composition. Separate bodies

of different major-element composition would not provide a plausible explanation of the correlation of petrography and chemistry since the simple gravitative settling process is quite sensitive to magma composition. Although we cannot exclude the possibility that some other process may be responsible for the correlation we intend to show that simple gravitative settling provides a quantitatively internally consistent explanation.

CRYSTAL SETTLING

We have done an experimental study of the crystallization of composition 12002 at controlled cooling rates (Walker *et al.*, 1976a). It was possible to specify the cooling history of sample 12002 at various points in its crystallization by comparison of petrographic and experimental olivine nucleation density, pyroxene "swallowtail" spacing, and groundmass grain size. We concluded that 12002 cooled through its liquidus ($\sim 1325^\circ\text{C}$) at $\sim 0.8^\circ\text{C/hr}$. and that the cooling rate subsequently decreased, so that about 2 months elapsed before the rock reached 1000°C . From this experimental work, the composition of the residual liquid and the degree of crystallinity are known as a function of temperature as are the sizes, shapes, and compositions of crystals which grow. From this information, viscosities, densities, and crystal settling velocities may be calculated as functions of temperature. This calculation is more practicable in the lunar case than in common terrestrial circumstances since there is no H_2O present and negligible Fe_2O_3 . The presence of either can have a considerable effect on the result, and their values can only be estimated in terrestrial magmas. Integration of the settling velocity over the time period

of the cooling history gives the distance some mineral is capable of settling. This measure of crystal mobility can be used to check whether the Apollo 12 olivine basalts can be genetically related by olivine fractionation in a magma body with cooling properties commensurate with the observations on 12002.

Table 2 lists the experimentally determined compositions of the residual liquid in 12002 as a function of temperature. Values at 50°C intervals were interpolated from graphs of composition versus quenching temperature. (Trends in the residual liquid compositions were very similar for all experiments cooled at $<50^\circ\text{C/hour}$.) The densities and viscosities of these residual liquids have been calculated according to the models of Bottinga and Weill (1970, 1972). Some calculations, however, require extrapolation of density and viscosity to lower temperatures ($<1200^\circ\text{C}$) than those covered by the models. In these cases the density and viscosity were calculated for the particular composition at high temperatures and extrapolated to lower temperatures. Density was taken to vary linearly with temperature; the natural logarithm of viscosity was varied linearly with inverse temperature. The density extrapolation involves relatively small changes in value and, therefore, probably small errors. The Arrhenius extrapolation probably tends to underestimate the viscosity at lower temperatures, thus leading to overestimates of settling velocities. However, as shown below for picritic liquids, most of the settling is over by the time the body has cooled to 1200°C , so these errors are taken to be minimal here.

The density variation of the residual liquid is quite small, decreasing from 3.29 to 3.26 g/cc between 1350°C and 1050°C. Evidently the change in chemistry favoring decreased density is nearly compensated by thermal contraction. The variation in viscosity (Figure 3) from ~10 poise near the liquidus to more than 1100 poise near the solidus is quite dramatic by contrast. Also shown in Figure 3 as functions of temperature are the degree of crystallinity (ϕ) of 12002 estimated optically and supported by crude chemical mass balances, the maximum size of olivines and the density of the olivines based on average core and rim compositions.

The settling velocity (V_s) of a sphere in a liquid is given by Stokes' Law as

$$V_s = \frac{2gr^2(\Delta\rho)}{9\eta} \quad (1)$$

where g is the acceleration of gravity (1.63 m/sec² on the moon), r is the radius of the sphere, $\Delta\rho$ is the density difference between the sphere and the liquid, and η is the viscosity of the liquid. Using this formula, settling velocities of olivines can be calculated as a function of temperature for the data shown in Figure 3. The results of these calculations are shown in Figure 4 where the temperatures are put on the time axis in a manner appropriate to the cooling history of 12002. The settling velocity rapidly increases with decreasing temperature from the liquidus to ~1250°C in response to the r^2 dependence of velocity on increasing crystal size. At lower temperatures the crystal has nearly attained its maximum size and the effects of logarithmically increasing

viscosity cause a rapid decrease in settling velocity. The area under the settling velocity curve corresponds to the total distance the growing crystal settles, which in this case is ~16 meters.

This simple calculation by Stokes' Law is not directly applicable to cooling magma bodies which are suspensions of non-spherical crystals. Shaw (1965) and Shaw *et al.* (1968) discuss some of the problems related to settling in silicate liquids. Shape factors (K) developed by McNown and Malaika (1950) can be used to correct symmetrical shapes for deviations from sphericity. However, for the case of nearly equant olivines produced at slower cooling rates no substantial correction is needed ($K = 1$). The fact that crystals are settling through a suspension of other crystals introduces non-trivial changes which are difficult to treat exactly. The viscosity of a pure liquid will be significantly different from that of a suspension of particles in the same liquid. Roscoe (1952) has extended the Einstein model for the bulk viscosity of a suspension to the case of unequal grain size distribution. When this model is applied to Stokes' Law, equation (1) becomes

$$V_{RE} = \frac{2gr^2(\Delta\rho)}{9K\eta}(1 - 1.35\phi)^{2.5} \quad (2)$$

where V_{RE} is the Roscoe-Einstein settling velocity, K is the shape factor and ϕ is the degree of crystallinity. When equation (2) is integrated over the cooling time there is a sharp decrease in the settling distance (relative to the simple

Stokes Law Calculation) to ~5.7 meters as shown in Figure 4. The presence of suspended crystals raises the effective viscosity and impedes settling.

An empirical expression for the settling of particles in a suspension has been developed by Lewis, Gilliland and Bauer (1949). When this expression is applied to Stokes' Law, equation (1) becomes

$$V_{LGB} = \frac{2gr^2(\Delta\rho)}{9K\eta}(1-\phi)^{4.65} \quad (3)$$

where V_{LGB} is the Lewis-Gilliland-Bauer settling velocity. Equation (3) is probably a more correct model than (2), since (2) is based upon the effective bulk viscosity of the suspension, rather than the effective viscosity experienced by a particle in the suspension. However, when V_{LGB} is integrated over time the settling distance is 4.1 meters, which is not very different from the integration of V_{RE} (5.7 meters). Thus we take the distance which olivine crystals may settle in a 12002 melt during the deduced cooling episode to be approximately 5 meters.

This estimate of ~5 meters is based upon a cooling rate which is initially 0.8°C/hour but progressively slows down and upon olivines which nucleate at the liquidus and reach 2 mm maximum dimensions. If the cooling rate is assumed to be a constant 0.8°C/hour, the settling distance based on V_{RE} changes from 5.7 to 5.3 meters. If the initial cooling rate is increased to 1.5°C/hour, the settling distance

based on V_{RE} drops to 2.7 meters. Obviously the calculation is much more sensitive to changes in the initial cooling rate than to changes in the form of the cooling curve because most of the settling occurs during the initial cooling of the magma. The calculation is also very sensitive to the size of the olivines. Few crystals in the natural specimen attain dimensions of 2 mm. Most olivines have a maximum dimension less than 1 mm. The smaller crystals have a computed settling distance of ~1 meter. It is clear that for the sort of cooling history inferred for 12002 the olivine crystals should have sunk out of any hand specimen-sized volume of melt in which they nucleated, no matter which calculation scheme is used.

An entirely different conclusion is reached when the calculations simulate the cooling of the vitrophyre, 12009 (Donaldson et al., 1975). Here the cooling rate after eruption is more uncertain (~500°C/hour). The olivines are platy and skeletal, which requires alteration of the shape factor ($K' = 2$) and density terms ($\Delta\rho' = \Delta\rho/2$). Strong composition gradients in the liquid make it difficult to estimate a meaningful value for the viscosity. However, even with these uncertainties the magnitude of the settling distances ranges only from 1 to 3 mm. Obviously these olivines do not settle out from their sites of nucleation and thus according to these calculations picritic liquids may certainly be preserved at very fast

cooling rates.

Another indication that these calculations give reasonable results in limiting cases can be found by calculating settling distances for pyroxenes in 12002. Experimentally grown pyroxenes did not attain the dimensions of the natural pyroxenes so a representative maximum dimension of 2 mm was taken from natural pyroxenes in thin section. An inferred size versus temperature plot is shown in Figure 3. For the cooling history of 12002, pyroxene settling in 12002 would amount to 3 to 5 cm. The results of the settling calculation appear in Figure 4. Pyroxenes would not be expected to settle far from their sites of nucleation. Whatever minor loss did occur from a particular volume would be readily compensated for by pyroxenes settling into that volume from above.* The great contrast between the settling distances predicted for olivines and pyroxenes is a result of the very large settling velocities of olivine near 1300°C where viscosity and crystallinity are low, whereas pyroxenes begin to grow and sink only after viscosity and crystallinity are substantially increased. As a result we should expect to find in the 12002 magma body considerable variation in the bulk rock chemistry as a result of olivine movements but little with respect to pyroxene. We noted above

*(Similar calculations also indicate that mobility of metal spherules, spinel, and plagioclase is very limited as a result of the small crystal sizes and large ϕ in the case of plagioclase.)

that the major-element chemistry of the olivine basalt suite is described by olivine control without significant pyroxene covariation. Apparently, simple olivine settling is at least qualitatively consistent with the differentiation which occurred in the natural magma both on the basis of chemistry and the experimentally determined physical properties of the magma.

The previous discussion has served to illustrate crystal settling calculations but must be substantially modified to calculate quantitatively differentiation by olivine settling. This is because as the crystals move they encounter new environments which are cooling more rapidly or more slowly than where they started. (The settling distances are large relative to hand specimen size.) We are required to consider more than just the cooling history at one point. To do this we must now investigate what can be said of the size and cooling history of the magma from which the samples came, and the probable sample distribution within that magma body.

MAGMA BODY CHARACTERISTICS

An important conclusion about the suite of samples can be drawn from considering the implications of the strong positive correlation of normative olivine with plagioclase grain size shown in Figure 2. In a magma body which differentiates by crystal settling, olivine accumulates at the bottom and is depleted at the top of the cooling unit. Cooling by heat loss to the

surroundings is more rapid at the margins and leads to a finer grain size at the margins relative to the interior of the body. These points are schematically indicated in Figure 2 for a thin magma body, e.g., flow or sill. Notice that only in the bottom portion of a cooling unit can one find a positive correlation of grain size and olivine abundance. The point is well illustrated in terrestrial examples such as the prehistoric Makaopuhi lava lake which has been described by Moore and Evans (1967, pp. 208-9). A question of some importance which this model must then face is: what has happened to the top of the magma body in which the Apollo 12 olivine basalts were generated? We will show from settling calculations that a substantial portion of this missing material will be depleted in olivine and have the composition of a cotectic residual liquid. O'Hara et al. (1975) have repeatedly pointed out the quantitative importance of cotectic residual liquid composition as a soil constituent. Perhaps the soil is the sink for this missing material. A possible explanation may be that meteorite impact selectively degrades the top portions of thick, differentiated picrite flows. Only the basal section (including a lower chill margin and some of the olivine cumulates) survives as samples large enough to be returned as hand specimens. Whether this degradation occurred in the time interval between flows at the Apollo 12 site or in the ~3 b.y. since the last flow there is conjectural. The answer to this question depends to a certain extent on what the stratigraphic order of flow types is

inferred to be and on the rate of soil production.

It should be noted that another mechanism is known for producing a positive correlation of olivine abundance with grain size. Drever and Johnston (1967a) have noted this relationship in some terrestrial sills where the correlation includes the top as well as the bottom of the cooling unit. If this situation applies, rather than the one analogous to the prehistoric Makaopuhi lava lake depicted in Figure 2, we are spared the embarrassment of finding the missing top of the Apollo 12 magma body. However, these cases are clearly related to magmas which were emplaced with substantial proportions of intratelluric phenocrysts since all parts of the body are more enriched in olivine than either the top or bottom chill margins, unlike the Makaopuhi case where the top of the lake is depleted in olivine relative to the chill margins. Bhattacharji (1967) has shown experimentally that intratelluric phenocrysts may be concentrated in the interior of flows and sills, relative to their chill margins, by flowage differentiation. Furthermore, Simkin (1967) has shown that the flowage differentiation mechanism is responsible for the distribution of olivine in the intrusions such as those illustrated by Drever and Johnston (1967a) to a much greater extent than simple olivine settling. An important feature of bodies in which olivine is distributed by flowage differentiation rather than simple settling is that olivine abundance correlates with olivine crystal size (in addition to the plagioclase grain size which is not controlled

by flowage differentiation). This is clearly seen in Simkin's (1967) profiles and is spectacularly sketched by Drever and Johnston (1967b). Olivine grain size variations of this magnitude (factor of ≥ 2 -3) are not seen in the Apollo 12 picrite suite and what little variation is present does not correlate with olivine abundance (Table 1). This suggests that we are not dealing with flowage differentiation in the Apollo 12 picrite suite. Furthermore, it will be shown below that settling would substantially modify a homogeneous initial distribution of intratelluric phenocrysts in an Apollo 12 picrite magma so that the final distribution would be quite unlike that observed. An initial distribution of phenocrysts concentrated toward the body center such as produced by flowage differentiation would make the resemblance even poorer. Sample 12009 was examined by Drever et al. (1972) for preferred orientation in its olivines such as might be expected from flowage differentiation. This quenched sample would be the most likely place to preserve such effects without later reorientation by settling. They did not regard their results as indicating any significant effect. We conclude the flowage differentiation model probably does not apply to the Apollo 12 picrites and will proceed with the simple settling model.

If this suite is a sampling of the bottom portion of a cooling unit, two rather important conditions apply to the history of the suite. The heat loss leading to solidification was principally through the adjacent magma bottom; and, as a result of cooling from below, the lower portions of the magma

body were gravitationally stable with respect to convection which would, then, not occur. These two conditions allow one to proceed with simplified thermal calculations--a conductive boundary (rather than fixed temperature or radiative surface appropriate to a flow top) may be used and convection may be neglected to a first approximation.

We may use the experimentally determined cooling history of sample 12002 to calculate how much insulation is necessary to hold this cooling element of magma to a certain initial cooling rate, i.e., how far away from the basal surface of heat loss the magma element must be to have that cooling rate. Estimates of the distance from this nearest surface of heat loss can then form the basis of an estimate of the dimensions of the magma body. Any perturbations introduced by surfaces of heat loss other than the nearest one will increase the cooling rate. If there are two surfaces of heat loss combining to give the observed cooling rate then those surfaces must be farther away to be equivalent in cooling power to a single surface of heat loss. Therefore, assuming only one nearby surface of heat loss (the base) and assigning all the conductive heat loss to that surface forms the basis for a minimum estimate of magma body size. The single-surface approximation will only be valid if the other surfaces of heat loss are several times as far away as the nearest one.

Therefore an estimate a few times the distance to the nearest surface of heat loss can be taken as a minimum estimate of the dimensions of the magma body.

An analytical treatment of this case which considers heat of fusion as well as a finite melting interval is due to Jaeger (1957), who improved upon the treatment of Winkler (1949). The solution for the distance from the base (x) has the form:

$$x = \sqrt{\frac{\xi}{\left(\frac{\partial T}{\partial t}\right)}} \quad (4)$$

where ξ is a proportionality constant given by a rather complicated expression involving the temperature range of solidification and the ratios of thermal diffusivities of magma and country rock. The diffusivities of magma and bedrock were taken to be the same ($0.01 \text{ cm}^2/\text{sec}$) except that the magma liberates latent heat of fusion (80 cal/gm) over a range of solidification from $1325\text{--}1000^\circ\text{C}$ which gives an effective diffusivity of the magma of only $0.0054 \text{ cm}^2/\text{sec}$ (viz., Jaeger's equation (1) on p. 307, 1957) for a specific heat of $0.29 \text{ cal/gm}\cdot\text{deg}$. The bedrock was taken to be initially at 0°C . To solve (4) for x , the value of the

cooling rate $\left(\frac{\partial T}{\partial t}\right)$ determined at the liquidus from olivine nucleation density of $\sim 0.8^\circ\text{C}/\text{hour}$ was used (Walker et al., 1976a). This value applies to the first 50°C or so of cooling (Walker et al., 1976b) and gives a value of ξ in (4) of $\sim 1.7^\circ\text{C}\cdot\text{cm}^2/\text{sec}$ when combined with the other constants above. The result is that 12002 is calculated to have crystallized about .90 m from the basal chill margin.

It is instructive to apply this same approach to the vitrophyre 12009 to determine its distance from a cooling surface. Donaldson et al. (1975) noted on the basis of crystal morphology and texture that the cooling rate upon eruption may have been greater than $100^\circ\text{C}/\text{hour}$. Walker et al. (1976a) suggested the rate may have been as much as $500^\circ\text{C}/\text{hour}$. Using these cooling rates and the thermal constants used above, adjusted for the lower liquidus (1250°C) of 12009, one calculates that x is 3-7 cm. Sample 12009 then is clearly part of the chill margin of its magma body, a conclusion in accord with its petrography.

It may be concluded then that the magma body of 12002 must have been several times a meter thick in minimum dimensions

according to the considerations discussed above. We point out that this conclusion is not dependent on accepting the notion that the suite comes from the bottom portion of a cooling unit. It is merely the solution that comes from a conductive boundary condition regardless of configuration. Analytical treatments which involve constant temperature heat-loss surfaces are also available (e.g., Carslaw and Jaeger, 1959, chapter 11) which would be appropriate to the upper surface of a lava flow. We find that this treatment places 12002 about 2.5 meters from such an exposed surface. 12002 was calculated to be closer to the conductive surface because the insulating country rock in such a configuration produces the same cooling rate with less intervening solidifying magma to act as an insulator. In either situation the 12002 magma body must have been at least several meters thick. It could be much larger also.

An important conclusion of our experimental study of 12002 (Walker *et al.*, 1976a) was that the cooling rate decreased with time during the solidification. The thermal calculations just described also indicate that the cooling rate should decrease. Specifically for 12002 the cooling rate is calculated to decrease by a factor of 3 between crystallization of liquidus olivine and groundmass and the solidification is calculated to take 3-4 weeks for the given initial cooling rate. We had previously guessed the rate might have decreased

by as much as a factor of 10 during the solidification (which might take a month or two). This was based on extrapolation of our experimental observations which were at cooling rates too rapid to cover all but the initial stages of 12002 crystallization.

Additional information on the cooling rates of the other samples in the suite would further our understanding of the dimensions of the magma body. Unfortunately no direct comparison of these samples with controlled cooling experiments is yet available, principally because the coarser samples require longer to cool than is presently feasible experimentally. Extrapolation of our experimental olivine nucleation density and pyroxene "swallow-tail" curves which indicate cooling rate is not useful since much of the olivine in the coarser samples is cumulus and the coarser pyroxene morphologies do not have recognizable "swallowtails." Fortunately, some progress can be made on the problem by considering groundmass plagioclase grain size.

GRAIN SIZE, COOLING RATE, AND MAGMA BODY SIZE

Although there are many complications which perturb the relation of grain size to cooling history and hence distance from the margin, sufficient terrestrial observations have been made to allow some cautious statements about the connection of the plagioclase grain size variation in our Apollo 12 suite and the size of the magma body.

Figure 5 shows plots of mineral grain size versus the measured distance from the margin of the body for a number of terrestrial occurrences of different minerals. As expected, grain size coarsens away from the body margins. What, then, is the

relationship that we may use to relate grain size to distance from the margin? To a first approximation the grain size could be considered to be linearly related to distance from the margin; however, if we consider the concavity towards the distance axis in Figures 5d, e, and f to be significant we might wish to formulate the relation as follows:

$$\text{size} \approx x^p \quad (5)$$

where p is an exponent less than or possibly near one. It is possible to estimate p from theoretical considerations as well as from Figure 5. From equation (4) we saw that distance (x) is inversely proportional to the square root of the cooling rate. This result is actually quite general and applies to many solutions of the cooling problem other than the specific one considered above. The relation of cooling rate and grain size is not so straightforward since it involves a complex interplay of diffusion, nucleation, and growth rates. However, we found experimentally that the spacing of growth instabilities in pyroxene, for example, displayed a linear relation with cooling rate on a log-log plot (Walker et al., 1976a, fig. 10). The slope of the line was $-\frac{1}{3}$:

$$\log(\text{size}) = -\frac{1}{3} \log(\text{cooling rate}) + b \quad (6)$$

which when combined with (4) gives $p = \frac{2}{3}$ in (5). We do not wish to claim that exponent $\frac{2}{3}$ is general or even correct. It is consistent with the relations in Figure 5 but only marginally, if at all, more so than a linear relation.

The grain size variation of plagioclase in the Apollo 12 olivine basalt suite may now be used to establish limits on the magma body size. Since we know the position of 12002 from experimental cooling studies (which give the cooling rate) and heat flow calculations (which give the position for that cooling rate) we can calibrate equation (5) for the suite:

$$\text{plagsize in mm} = .004 (\text{distance in cm})^{2/3} \quad (7)$$

or

$$\text{plagsize in mm} = .089 (\text{distance in m}) \quad (8)$$

depending on choice of exponent. The parallel studies on 12009, the vitrophyre, afford a cross check on which exponent is appropriate. Using (7) and data in Table 1, 12009 is calculated to be $\frac{1}{3}$ cm from the margin; and using (8) the distance is $2\frac{1}{4}$ cm. It would seem that (8) the linear relation, gives slightly better internal consistency. Lane (1903b) suggested theoretical reasons why the relation might be linear if equation (4) applies. We adopt (8) which gives the most conservative size estimates.

The coarsest samples represent those furthest from the base of the body and they are calculated to be .11 meters from the base by (8). [The distance would be .38 meters by (7).] The magma body must be at least a few times this distance in thickness so that heat loss from the top surface does not contribute to a more rapid cooling history than implied. The coarse gabbros come from a magma body that was probably at least 30 meters in thickness. Although flows of this thickness are known (Schaber et al., 1976) there is also evidence that lunar

REPRODUCIBILITY OF THE ORIGINAL PAGE IS POOR

lava flows are commonly thinner. Brett (1975) summarized this evidence and argued by similar reasoning connecting chemical kinetic and heat flow data that most lunar lava flows were probably less than 10 meters in thickness. Although no kinetic data on these coarse gabbros was available to Brett and hence there is no direct conflict, coarse gabbros from Apollo 15 gave solutions placing them in surprisingly thin flows (e.g., 15065). An analysis based on plagioclase grain size would probably place them in substantially thicker flows. Brett's analysis was based on Zr partitioning between ulvöspinel and ilmenite which Taylor et al. (1973) have shown to be related to cooling rate. The temperature range covered by this analysis is large--down to 850°C. Winkler (1949, p. 563) noted that when temperature falls substantially below the temperature of intrusion (e.g., to 850°C here) cooling rate differences across an intrusive are small. If the Zr partitioning is responding well down to these subsolidus temperatures then the reason coarse and fine-grained samples give similar cooling rates by Zr partitioning is understood. In this case, cooling rates determined from features developed within the solidification range will be a more reliable indicator of position within a magma body than features developed in the subsolidus. Therefore we tentatively prefer to use the analysis based on plagioclase grain size even though it implies substantially thicker magma bodies than previous studies indicated. Recognition of uncertainties, especially those associated with possible boundary conditions such as layers of

soil of low thermal conductivity, may make the results of the different calculations more compatible. Table 1 lists distances calculated on the basis of equation (8) and these are used in Figure 8.

MAGMA DIFFERENTIATION

We now wish to explain quantitatively the distribution of olivine in the Apollo 12 olivine basalt suite on the basis of gravitative olivine settling into the bottom portion of the magma body which the suite of samples represent. The explanation will be satisfactory if it can produce the curve of Figure 8 which gives olivine concentration as a function of distance above the base. The simplest interpretation of this curve is that 12009, the vitrophyre at the chill margin, represents the magma bulk composition in which the accumulation has occurred. In this interpretation 12002 would be a phenocryst-enriched liquid rather than a liquid composition.*

*The amount of cumulus olivine suggested from Figure 2 and Table 1 is about 9% based on an average normative olivine content for 12002 from two different analyses. Our analysis of 12002, 57 (the sample crystallized experimentally) suggests that it has only $4\frac{1}{2}\%$ more normative olivine than 12009. The difference in analyses may reflect heterogeneity in olivine phenocryst content as noted above for 12004. Furthermore, from the data in Table 1 of Walker et al. (1976a) it can be calculated that $3\frac{1}{2}\%$ of cumulus olivine in 12002 would explain the difference

It will be assumed that 12009 is a better guide to initial magma composition. This assumption and other alternatives will be considered later.

The calculation of olivine settling profiles is done by computer. A size is postulated for the magma body. At the liquidus temperature olivine crystals are allowed to nucleate at arbitrary even spacings. The magma cooling is computed and the crystals grow and settle. The computation for each crystal stops when the velocity becomes negligible. The olivine concentration in the final settling profile is computed by considering how close the final positions of the crystal are relative to their initial spacing. This follows the convenient formulation of Fujii (1974).

Settling velocities are computed from equation (3). The input parameters as a function of temperature are determined from the experimental work on 12002 as shown in Figure 3. Olivine radius is not taken from Figure 3, which gives the maximum experimental olivine sizes. Instead olivine was allowed to grow to sizes representative of the olivines

in composition between the experimental liquidus olivine (Fo₇₈) and the olivine actually present in the sample (Fo₇₆). A few percent cumulus olivine in 12002 makes little difference in the cooling rate cited above since the cumulus olivine can be accounted for by a few large crystals. The nucleation density, therefore, changes little; moreover, the cooling rate estimate is rather insensitive to nucleation density in this range of cooling rates.

petrographically observed in the suite (Table 1) with a temperature dependence of size as shown in Figure 3. Various sizes were used. Also, for some calculations it was assumed that olivine was present in suspension at the time of intrusion and settling of these phenocrysts, without further growth, was calculated.

For calculation purposes the magma body was assumed to be a flow with upper surface at 0°C and the heat flow solution of Jaeger (1968) was used to determine temperature as a function of time and position:

$$T = T_0 \left\{ \frac{1}{2} \operatorname{erf} \frac{x+a}{2\sqrt{kt}} - \frac{1}{2} \operatorname{erf} \frac{3a-x}{2\sqrt{kt}} - \operatorname{erf} \frac{x-a}{2\sqrt{kt}} \right\} \quad (9)$$

where x is the distance from the midplane of the flow with thickness $2a$, T_0 is the extrusion temperature (1250°C for a magma with 12009 properties), t is time, erf is the error function, and k is the thermal diffusivity (0.01 cm²/sec). This solution does not consider liberation of latent heat and the thermal properties of the magma and bedrock are assumed to be the same. We shall see later that certain results of the calculations allow use of a solution which does include the effects of liberation of latent heat.

In order to make computing time manageable, but at the same time keep the final computed position of the crystals numerically stable, it was necessary to make the time steps in the iterative calculation adjustable. This is especially important when the sinking crystal encounters a regime of rapidly changing settling velocity. The procedure adopted was to compare the velocity at the start of a time step with that at the end of the time step at the new, tentative, position of the crystal. If the positions of the crystal computed with the different velocities disagreed by more than

500 microns, the crystal was not advanced to the new position and the time step was halved until the computed positions at the end of the time step differed by less than 500 microns. If the difference in final positions was less than 50 microns, the time step was doubled for the next step and tested again. It was found that decreasing the maximum permissible difference to 100 microns did not change the final calculated positions of the crystals.

Figure 6 shows some calculated settling profiles for a spectrum of magma sizes and for various different ultimate sizes for the growing olivines. Olivine concentration is plotted as a function of position in the bodies. One obvious feature of these profiles is that larger bodies differentiate more than small ones as would be expected since larger bodies cool more slowly and allow more settling before solidification. For 6a and b where crystals grow during solidification, a 1-meter flow cools too rapidly to experience any differentiation whereas a 64-meter thick flow settles all olivine out of a substantial portion of its interior. For the case of olivine crystals growing to a maximum radius of $\frac{1}{2}$ mm (6b) more settling occurs than for a maximum radius of $\frac{1}{3}$ mm (6a). The profile is thus very sensitive to crystal size. As we noted before in the section on crystal settling, most of the settling occurs at temperatures very near the liquidus. If the magma is extruded with a suspension of phenocrysts already developed,

the settling velocity is at a maximum at first extrusion since these crystals do not have to grow to sizes large enough to settle rapidly. Figure 6c shows profiles computed for the case of phenocrysts of $\frac{1}{3}$ mm radius extruded with the magma and allowed to settle without further growth. There is obviously a dramatic increase in settling compared to 6a and b even though the crystals in 6b grow to larger size. The profile is therefore even more sensitive to crystal size near the extrusion temperature than to the final growth size.

One feature exhibited by 6c and common to all the profiles we computed for original suspensions of phenocrysts, is the roughly linear slope on the portion of the curve near the magma bottom. In some cases the curve is actually slightly concave towards the concentration axis (e.g., fig. 7a). This behavior contrasts with profiles calculated for crystals growing during settling which are convex towards the concentration axis near the magma bottom although some approach linearity. It is to be noted that the olivine concentration versus distance curve for the Apollo 12 suite (figure 8) is distinctly convex towards the concentration axis. The simplest explanation is that this suite represents accumulation of crystals which mostly grew after extrusion rather than accumulation of a suspension of phenocrysts developed prior to emplacement.

Another feature of the profiles is that zones of extreme olivine concentration develop complementary to zones completely

devoid of olivine. Since no provision was made in the calculations to avoid mutual interference of olivine crystals, these olivine-enriched horizons which develop are unrealistically thin and concentrated. An olivine concentration factor of 5 is probably about the realistic physical limit possible and the curves are arbitrarily cut off there. No attempt was made to estimate realistic thickness for these olivine-enriched zones since none appear to have been sampled (no dunites) and our principal concern here is the section adjacent to the base and beneath the zone of greatest olivine enrichment.

An important feature of the profiles in figure 6 is obscured by the presentation of many different magma body sizes on a scaled distance coordinate. For any particular set of conditions (e.g., crystal size, extrusion temperature, etc.) the olivine concentration curve near the magma bottom is independent of magma size. The curves for different size bodies overlap until the curve for the smaller body either develops a highly concentrated zone or falls back to lower concentrations. This feature is observed for every spectrum of magma body sizes for every condition we calculated. Two examples are shown in figure 7. This result is intuitively plausible when one considers that the settling which occurs near the margin will be controlled by the heat loss at that margin. For regimes near the margin this initial heat loss is independent of the size of the magma body. We have argued that the Apollo 12 olivine basalt

suite does sample such a regime near the magma base. If this is true then we can calculate the settling profile for the lower portion of a magma body large enough to include the Apollo 12 olivine basalt suite as this lower zone with an analytical heat flow solution which includes the effect of latent heat.

We used such a solution (Jaeger, 1957) in the discussion above relating cooling rate to distance from the base, and it can be applied here also:

$$T = \frac{T_S - T_L \cdot \gamma}{1 - \gamma} + \frac{T_L - T_S}{1 - \gamma} \operatorname{erf} \frac{x}{2\sqrt{kt}} \quad (10)$$

T_L (1250°C) and T_S (1000°C) are the liquidus and solidus temperatures; x is the distance from the base; t is the time; k is the effective diffusivity of the magma when a latent heat of 80 cal/gm is liberated uniformly over the solidification range (here taken as 0.0048 cm²/sec); and γ is a complicated expression involving the solidification temperatures and ratio of effective diffusivities of magma and country rock (with a numerical value here of 0.546).

Settling profiles for the bottom of a magma were then calculated with this formula for a large magma thickness (arbitrarily taken as 64 meters). These are shown in figure 8(a and b). The consideration of latent heat makes a noticeable difference to the settling profile. Figures 6a and b show dashed curves calculated this way for comparison to calculations without latent heat. Settling and concentration at the base is enhanced

in these models as compared to those which do not take latent heat into account. The inclusion of latent heat undoubtedly, gives a more realistic result. We repeated the set of calculations for a magma with 12002 physical properties ($T_L=1325^\circ\text{C}$; $k=.0054$ cm²/sec; $\gamma=.456$) to check the relative merits of the two magma compositions. The higher liquidus temperature of 12002 with slightly more normative olivine results in increased settling for any particular crystal size. (See curve 8c.)

Also plotted in Figure 8 is the Apollo 12 olivine basalt suite. It is clear that the settling profile for olivines growing to a radius of $\frac{1}{2}$ mm in a magma with 12009 extrusion temperature (1250°C) and composition gives a very good description of the Apollo 12 olivine basalt suite for the upper part of the curve. However, the suite seems to have concentrated slightly more olivine in its basal members than would be expected for a 12009 magma composition. On the other hand, a 12002 magma composition will concentrate too much olivine in its basal section to be consistent with the Apollo 12 olivine basalt suite. This may indicate either that the actual magma was intermediate between 12002 and 12009, that a small fraction of the olivine in a 12009 magma was present at the time of emplacement as phenocrysts, or that some combination of these effects may have operated. In either case, the deviations of the suite from the calculated profiles are rather small.

We conclude that simple olivine settling can give a quantitative, internally consistent explanation for the chemical and petrographic properties of the Apollo 12 olivine basalt suite.

ACKNOWLEDGEMENTS

This work was supported by NASA Grant NGL 22-007-247 and the Committee on Experimental Geology and Geophysics of Harvard University. We thank R. Brett, R. T. Helz, and T. L. Wright for valuable comment and criticism of an earlier draft of parts of this work. Review suggestions of R. Brett, R. H. Hewins, and P. Weiblen have improved the present version. We offer them our thanks.

REFERENCES

- Bhattacharji S. (1967) Scale model experiments on flowage differentiation in sills., in Ultramafic and Related Rocks, p. 69-70, P. J. Wyllie, editor, Wiley, New York.
- Bottlinga Y. and Weill D.F. (1970) Densities of liquid silicate systems calculated from partial molar volumes of oxide components. Am. Journ. Sci. 269, p. 169-182.
- Bottlinga Y. and Weill D.F. (1972) The viscosity of magmatic silicate liquids: a model for calculation. Amer. Jour. Sci. 272, p. 438-475.
- Brett R. (1975) Thickness of some lunar mare basalt flows and ejecta blankets based on chemical kinetic data. Geochim. Cosmochim. Acta 39, p. 1135-1141.
- Carslaw H.S. and Jaeger J.C. (1959) Conduction of heat in solids, 2nd ed. Oxford University Press.
- Compston W., Berry H., Vernon M.J., Chappell B.W., and Kaye M.J. (1971) Rb-Sr chronology and chemistry of lunar material from the Ocean of Storms. Proc. Lunar Sci. Conf. 2nd, p. 1471-1485.
- Cuttitta F., Rose H.J. Jr., Ansell C.S., Carron M.K., Christian R.P., Dwornik E.J., Greenland L.P., Helz A.W., and Ligon D.T. Jr. (1971) Elemental composition of some Apollo 12 lunar rocks and soils. Proc. Lunar Sci. Conf. 2nd, p. 1217-1229.
- Donaldson C.H., Usselman T.M., Williams R.J., and Lofgren G.E. (1975) Experimental modeling of the cooling history of Apollo 12 olivine basalts. Proc. Lunar Sci. Conf. 6th,

p. 843-869.

- Drever H.I. and Johnston R. (1967a) The ultra-basic facies in some sills and sheets., in Ultramafic and Related Rocks, p. 51-63, P.J. Wyllie, editor, Wiley, New York.
- Drever H.I. and Johnston R. (1967b) Picritic minor intrusions., in Ultramafic and Related Rocks, p. 71-82, P.J. Wyllie, editor, Wiley, New York.
- Drever H.I., Johnston R., Butler P. Jr., and Gibb F.G.F. (1972) Some textures in Apollo 12 lunar igneous rocks and in terrestrial analogs. Proc. Lunar Sci. Conf. 3rd, p. 171-184.
- Engel A.E.J., Engel C.G., Sutton A.L., and Myers A.T. (1971) Composition of five Apollo 11 and Apollo 12 rocks and one Apollo 11 soil and some petrogenetic considerations. Proc. Lunar Sci. Conf. 2nd, p. 439-448.

- Fujii T. (1974) Crystal settling in a sill. Lithos 7, 133-137.
- Green D.H., Ware N.G., Hibberson W.O., and Major A. (1971) Experimental petrology of Apollo 12 basalts: Part 1, Sample 12009. Earth Planet. Sci. Lett. 13, 85-96.
- Grove T.L., Walker D., Longhi J., Stolper E., and Hays J.F. (1973) Petrology of rock 12002 and origin of picritic basalts at Oceanus Procellarum. Proc. Lunar Sci. Conf. 4th, 995-1011.
- Hodges F.N. and Papike J.J. (1975) Mare basalts: petrology (abstract). In Origins of mare basalts and their implications for lunar evolution, pp. 72-76. The Lunar Science Institute, Houston.
- Jaeger J.C. (1957) The temperature in the neighborhood of a cooling intrusive sheet. Amer. Jour. Sci. 255, 306-318.
- Jaeger J.C. (1968) Cooling and solidification of igneous rocks. In Basalts, the Poldervaart treatise on rocks of basaltic composition, edited by H.H. Hess and A. Poldervaart, Interscience, N.Y.
- James O.B. and Wright T.L. (1972) Apollo 11 and 12 mare basalts and gabbros: classification, compositional variations, and possible petrogenetic relations. Geol. Soc. Am. Bull. 83, 2357-2382.
- Kushiro I. and Haramura H. (1971) Major element variation and possible source materials of Apollo 12 crystalline rocks. Science 171, 1235-1237.

- Lane A.C. (1903a) Studies of the grain of igneous intrusives. Geol. Soc. Am. Bull. 14, 369-384.
- Lane A.C. (1903b) Porphyritic appearance of rocks. Geol. Soc. Am. Bull. 14, 385-406.
- Laughlin A.W., Brockins D.G., and Carden J.R. (1972) Variations on the initial Sr ratios of a single basalt flow. Earth and Planet. Sci. Lett. 14, 79-82.
- Lewis W.K., Gilliland E.R., and Bauer W.C. (1949) Characteristics of fluidized particles. Indust. Eng. Chem. 41, 1104-1117.
- Maxwell J.A. and Wilk H.B. (1971) Chemical composition of Apollo 12 lunar samples 12004, 12033, 12051, 12052, 12065. Earth and Planet. Sci. Lett. 10, 285.
- McNown J.S. and Malaika J. (1950) Effects of particle shape on settling velocity at low Reynolds numbers. Amer. Geophys. Union. Trans. 31, 74-82.
- Moore J.G. and Evans B.W. (1967) The role of olivine in the crystallization of the prehistoric Makaopuhi tholeiitic lava lake, Hawaii. Contr. Min. Pet. 15, 202-223.
- O'Hara M.J., Humphries D.J., and Waterston S. (1975) Petrogenesis of mare basalts: implications for chemical, mineralogical, and thermal models for the moon. Proc. Lunar Sci. Conf. 6th, 1043-1055.
- Queneau A.L. (1902) The size of grain in igneous rocks in relation to the distance from the cooling wall. The School of Mines Quarterly 23, 181-194, Columbia University, N.Y.

- Roscoe R. (1952) The viscosity of suspensions of rigid spheres. Brit. Jour. Appl. Physics 3, p. 267-269.
- Schaber G.G., Boyce J.M., and Moore H.J. (1976) The scarcity of mappable flow lobes on the lunar surface: unique morphology of the Imbrium flows (abstract). In Lunar Science VII, p. 767-769. The Lunar Science Institute, Houston.
- Schoon H.J. (1971) Chemical analyses of lunar samples 12040 and 12064. Proc. Lunar Sci. Conf. 2nd, p. 1259-1260.
- Shaw H.R. (1965) Comments on viscosity, crystal settling, and convection in granite magmas. Amer. Jour. Sci. 263, p. 120-152.
- Shaw H.R., Wright T.L., Peck D.L., and Okamura R. (1968) The viscosity of basaltic magma: an analysis of field measurements in Makaopuhi lava lake, Hawaii. Amer. Jour. Sci. 266, p. 225-264.
- Simkin T. (1967) Flow differentiation in the picritic sills of northern Skye., in Ultramafic and Related Rocks, p. 64-69, P.J. Wyllie, editor, Wiley, New York.
- Taylor L.A., McCallister R.H., and Sardi O. (1973) Cooling histories of lunar rocks based on opaque mineral geothermometers. Proc. Lunar Sci. Conf. 4th, p. 819-828.
- Walker D., Kirkpatrick R.J., Longhi J., and Hays J.F. (1975) 12002 revisited (abstract). In Lunar Science VI, p. 841-843. The Lunar Science Institute, Houston.
- Walker D., Kirkpatrick R.J., Longhi J., and Hays J.F. (1976a) Crystallization history of lunar picritic basalt sample 12002: phase equilibria and crystallization history.

Soc. Am. Bull., v. 87, p. 646-656.

Walker D., Kirkpatrick R.J., Longhi J., and Hays J.F. (1976b)

Olivine nucleation in lunar basaltic melts in iron capsules (abstract). EOS 57, p. 356.

Walker F. (1940) Differentiation of the Palisades diabase,

New Jersey. Geol. Soc. Am. Bull. 51, p. 1059-1106.

Walker K.R. (1969) The Palisades sill, New Jersey: a reinvestigation. Geol. Soc. Am. Spec. Pap. 111.

Warner J.L. (1971) Lunar crystalline rocks: petrology and geology. Proc. Lunar Sci. Conf. 2nd, p. 469-480.

Willis J.P., Ahrens L.H., Danchin R.V., Erlank A.J., Gurney J.J.,

Hofmeyr P.K., McCarthy T.S., and Orren M.J. (1971) Some interelement relationships between lunar rocks and fines, and stony meteorites. Proc. Lunar Sci. Conf. 2nd, p. 1123-1138.

Winkler H.G.F. (1949) Crystallization of basaltic magma as recorded by variations of crystal size in dikes. Min. Mag. 28, p. 557-574.

TABLE 1

APOLLO 12 OLIVINE BASALT DATA

	<u>12009</u>	<u>12075</u>	<u>12004</u>	<u>12002</u>	<u>12020</u>	<u>12018</u>	<u>12040</u>	<u>12035</u>
* modal olivine	13.6	18.2	11.9	19.6	14.3	14.1	24.6	28.7
* range of Fo in olivine	76-49	77-51	76-54	77-50	77-32	76-49	67-44	63-50
† normative olivine content	12.3	17.5	17.9	21.6	20.5	25.4	27.4	30.9
* mineral size in mm:								
plagioclase	.002	.05	.06	.08	.11	.16	.46	.98
olivine	.56	.77	.53	.72	.60	.63	.72	.51
* distance in meters above base	.02	.56	.67	.90	1.2	1.8	5.2	11.0

* Average values from 1 to 3 sections of each rock. Samples used were: 12009,14; 12075,24; 12004,51; 12002,7,9, and 160; 12020,8 and 15; 12018,6,77, and 79; 12040,44 and 45; 12035,21 and 22.

† Average of values from analyses reported by: Compston et al. (1971), Cuttitta et al. (1971), Engel et al. (1971), Grove et al. (1973), Kushiro and Haramura (1971), Maxwell and Wiik (1971), Schoon (1971), and Willis et al. (1971). Table 10 of James and Wright (1972) gives a convenient compilation.

* Calculated by equation (8) in the text from plagioclase size.

TABLE 2

FRACTIONATED RESIDUAL LIQUIDS

T°C	1350	1300	1250	1200	1150	1100	1050
SiO ₂	43.7	43.8	44.3	45.0	46.0	46.7	46.5
TiO ₂	2.5	3.0	3.3	3.5	3.8	4.2	4.5
Al ₂ O ₃	8.0	8.5	9.5	10.0	11.5	12.5	14.0
Cr ₂ O ₃	0.70	0.85	1.0	0.6	0.3	0.15	0.07
FeO	21.9	21.3	21.1	20.4	19.3	18.9	19.6
MgO	13.5	11.4	9.8	8.2	6.1	4.1	2.7
CaO	8.0	8.7	9.5	10.1	10.8	11.1	10.8
K ₂ O	0.05	0.06	0.07	0.07	0.08	0.09	0.10
Na ₂ O	<u>0.23</u>	<u>0.27</u>	<u>0.30</u>	<u>0.33</u>	<u>0.36</u>	<u>0.40</u>	<u>0.45</u>
	98.58	97.88	98.87	98.20	98.24	98.14	98.72

Residual liquid compositions interpolated from experimental comparisons of residual liquids produced at cooling rates < 50°C/hour. K₂O and Na₂O values necessary for the viscosity and density calculations are estimated from initial bulk content and degree of crystallinity. This disequilibrium fractionation trend may be compared to the equilibrium sequence in table 1 of Walker *et al.* (1976a).

FIGURE CAPTIONS

Figure 1

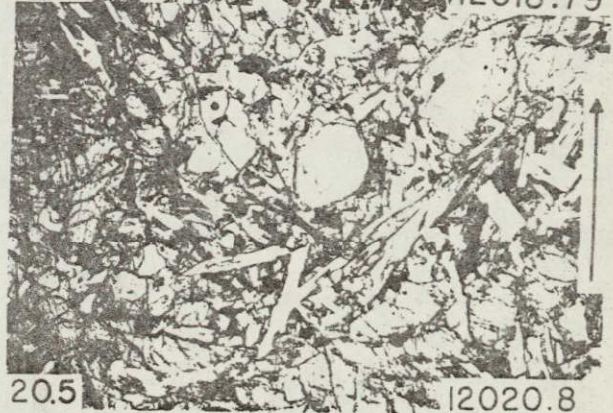
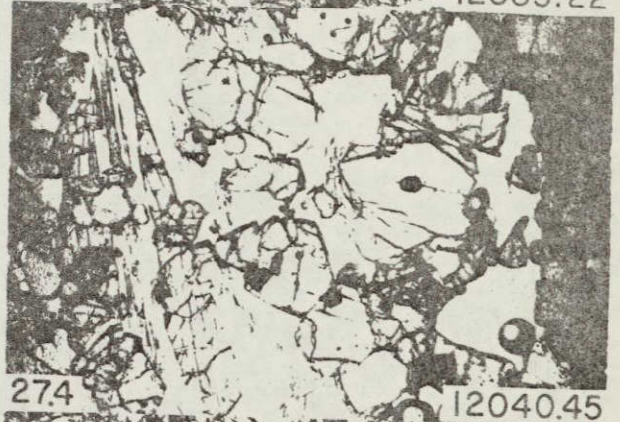
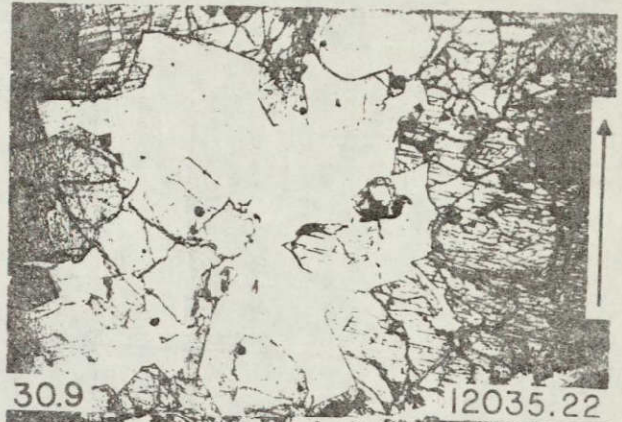
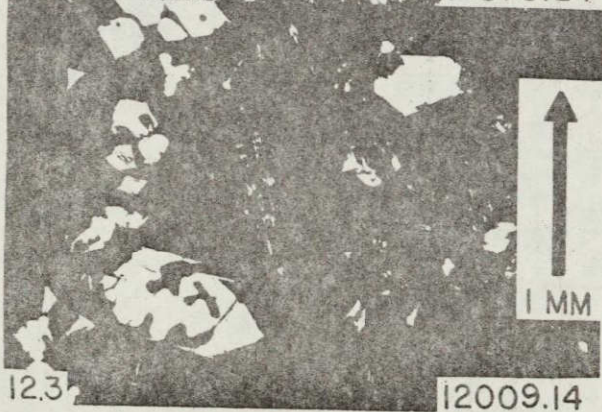
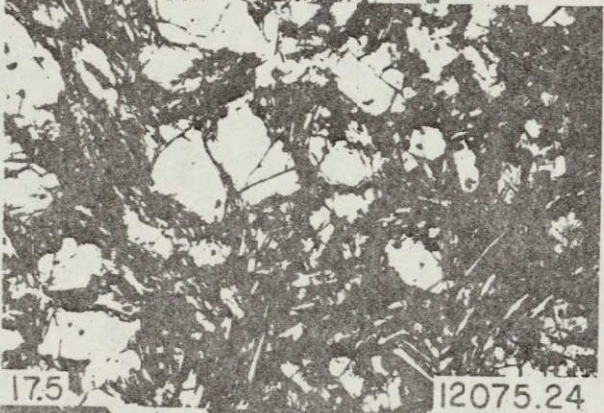
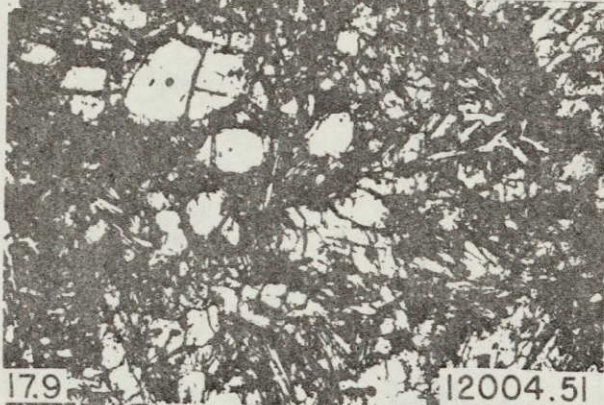
Photomicrographs in transmitted light. Numbers in lower left of each frame are normative olivine contents from Table 1; in lower right are the section sample numbers. Arrows indicate the progression away from the inferred base of the sequence and are 1 mm long. (All photos at same scale.)

Figure 2

Average plagioclase size, measured as the width of large laths, is plotted against average normative olivine content from Table 1. Error bars indicate ranges from different sections and different analyses listed in Table 1. Schematic diagrams beneath indicate a positive correlation of these variables may be expected at the bottom of a cooling unit differentiating by olivine settling.

Figure 3

The variation in physical properties as a function of temperature is shown for 12002 during crystallization at rates less than 50°C/hour. Liquid viscosity is calculated by the model of Bottinga and Weill (1972). Olivine density is estimated from average olivine compositions. Crystal size is the maximum observed in experimental olivines. Pyroxene size is estimated on the basis of growth to a 2 mm maximum size. ϕ is the degree of crystallinity. These values for the physical properties are used to calculate crystal settling



REPRODUCIBILITY OF THE ORIGINAL PAGE IS POOR

velocities shown in Figure 4.

Figure 4

Calculated settling velocity for olivine and pyroxene is shown throughout the 12002 crystallization history as calculated by various methods discussed in the text. Note that the velocity scale for pyroxene is much expanded relative to that for olivine. Areas under the curves are a measure of how far olivine or pyroxene can settle. These distances are given in parentheses after the symbol indicating which formula was used to calculate the curve.

Figure 5

Plots of linear dimensions of minerals versus their distance from cooling surfaces. Literature sources are: Lane (1903a), Moore and Evans (1967), Queneau (1902), and F. Walker (1940). Queneau's data is plotted as the square root of area reported. F. Walker's data for plagioclase in the olivine diabase horizon of the Palisades sill is indicated in separate symbols since K. R. Walker (1969) has shown that this material (and what is above) is involved in a second magma injection which perturbs a simple cooling history. Queneau evidently avoided this material in his analysis.

Figure parts a, b, and c include data only from the marginal facies of the solidified bodies. The plots are more nearly linear than parts d, e, and f where the observations include material at the center of the body. The marginal

portions of d, e, and f can be considered approximately linear. The curvature of plots d, e, and f reflects the additive cooling effects of both margins on the grain size in the body center.

Parts a, c, and d include data from more than one section across the bodies and indicate the sort of lateral variations that may be found in a body. All the minerals compiled here are thought to have crystallized after magma emplacement (with the possible exception of those in part f) and the patterns here should not be influenced by flowage differentiation during magma emplacement.

Figure 6

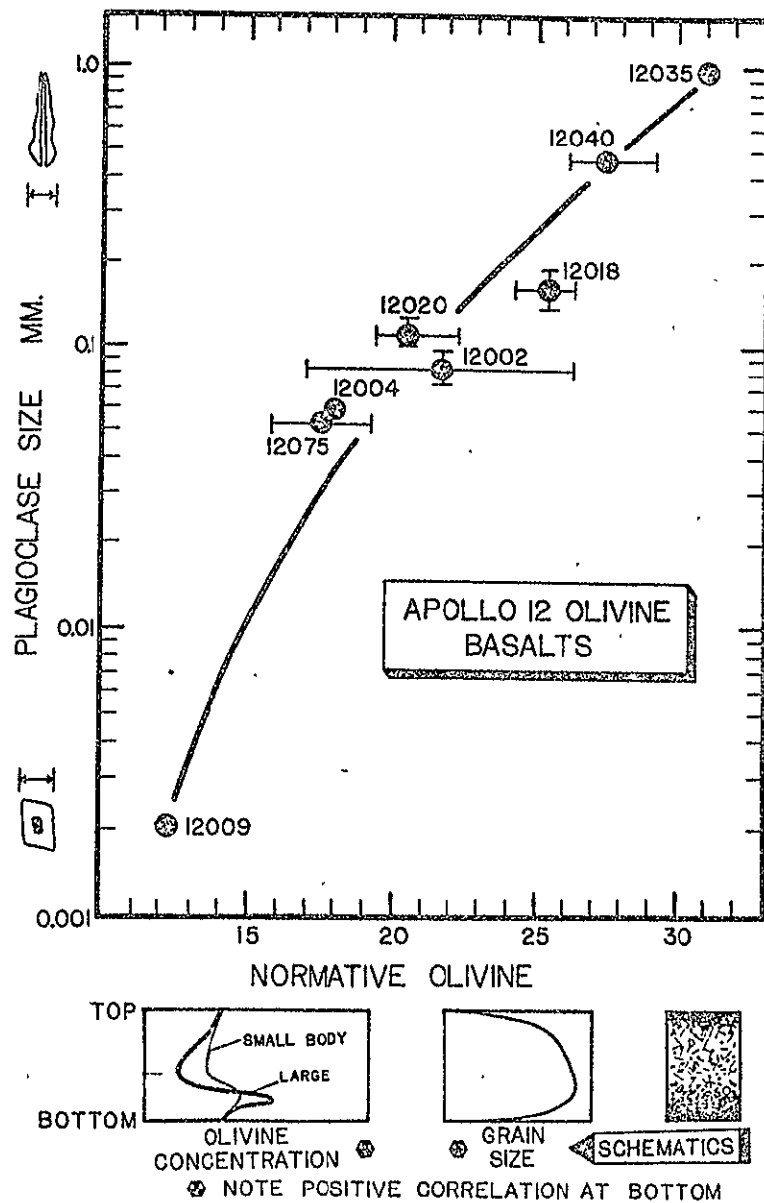
Calculated profiles of olivine settling for flows of various thickness. Vertical position coordinate is scaled for total thickness which is indicated in meters by the circled numbers. The olivine concentration scale on the abscissa is relative; unity is the initial value for each of the magmas which are assumed to be homogeneous liquids or homogeneous crystal-liquid mixtures at time of emplacement. Equation (9) gives temperature history. Dashed curves in lower portions of a and b give results from equation (10) for comparison of effect of latent heat on a 64 meter thick flow. Results in a and b are for crystals which grow during settling as contrasted to c where phenocrysts of $\frac{1}{3}$ mm radius are present at time of emplacement, and do not grow during settling.

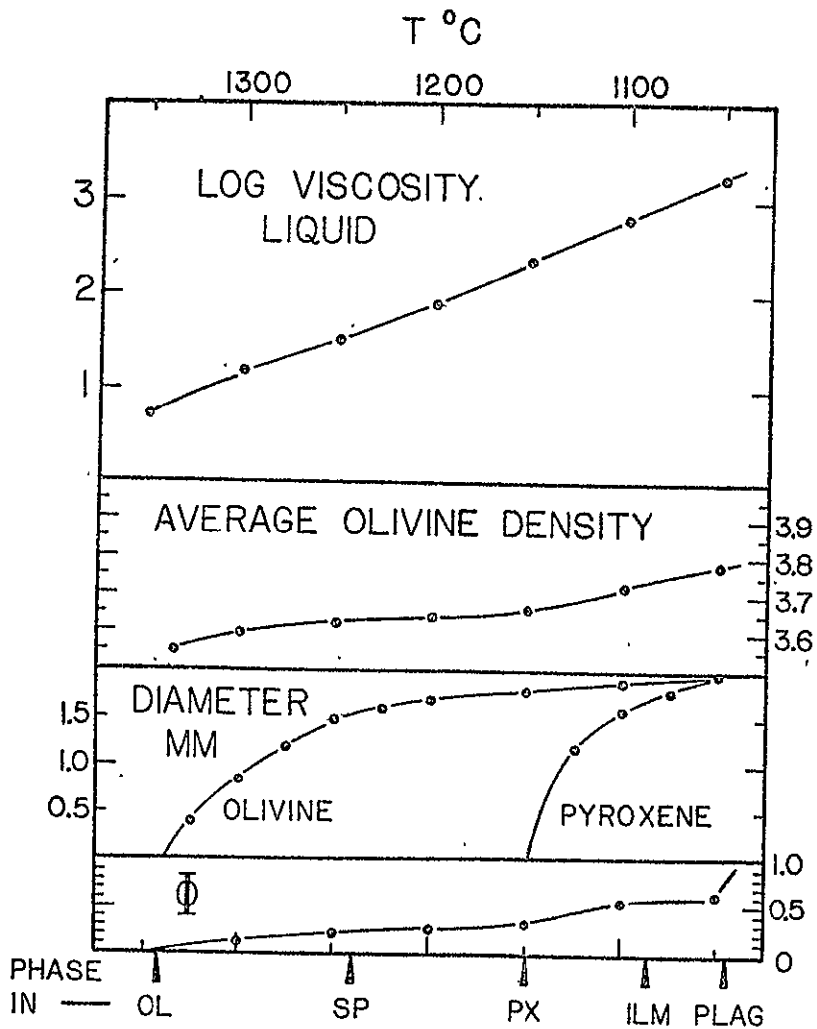
Figure 7

Calculated profiles of olivine settling. Vertical position coordinate covers basal 2 meters of flows, so only the bottom of flows thicker than 2 meters are shown. Olivine concentration scale is same as for Figure 6. Note the coincidence of curves until curves either indicate beginning of depleted zone or concentrated zone. Note contrast in shape for the coincident portion of the curves. Calculations for olivines of constant radius present during initial emplacement (a) are slightly concave downwards. Calculations for olivines which grow during settling (b) are convex downwards.

Figure 8

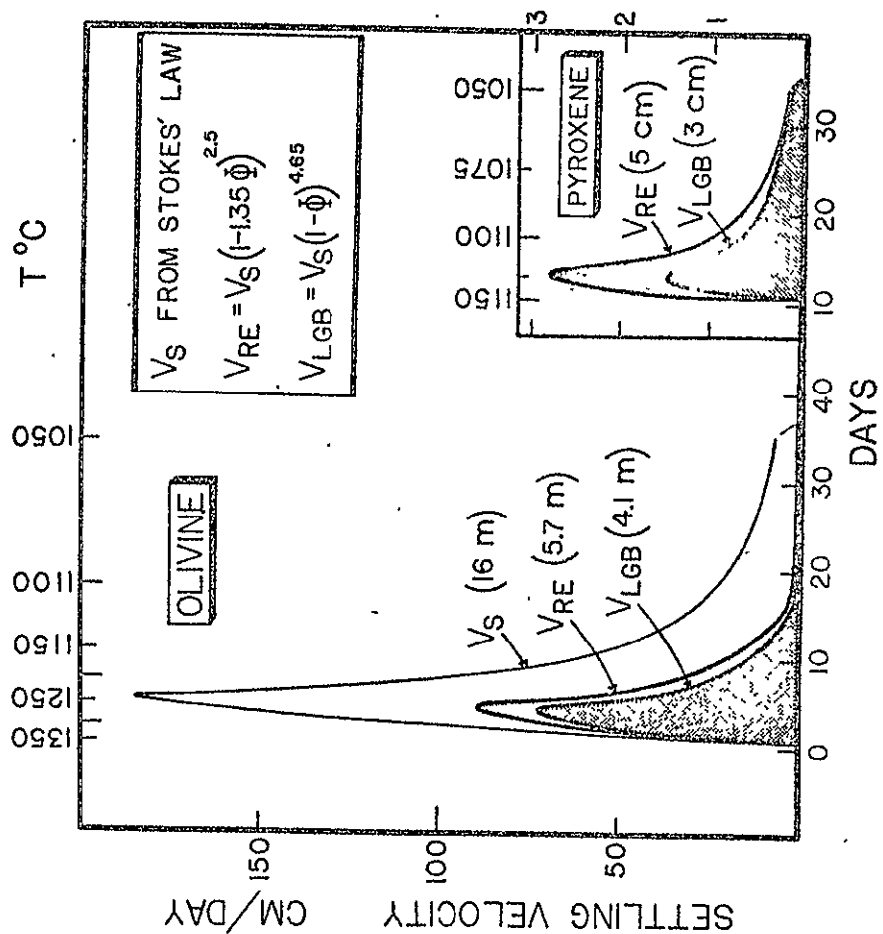
Apollo 12 olivine basalt suite is placed according to data in Table 1 and equation (8), and compared to calculated settling profiles. These profiles are for the base of a large magma body and incorporate the effect of latent heat by equation (10).

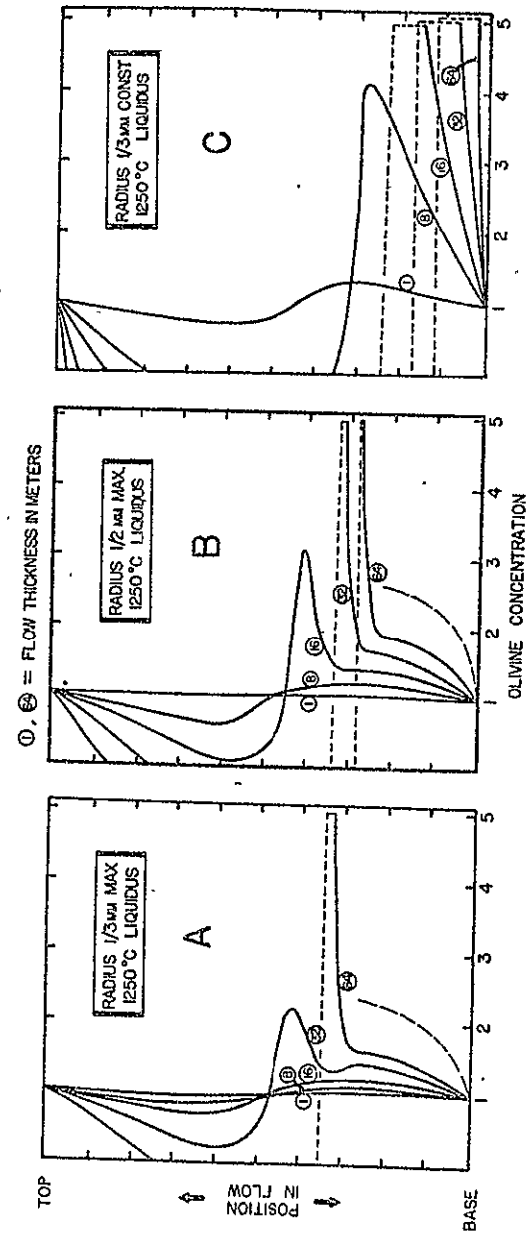
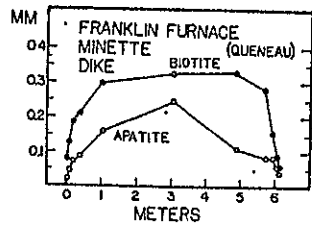
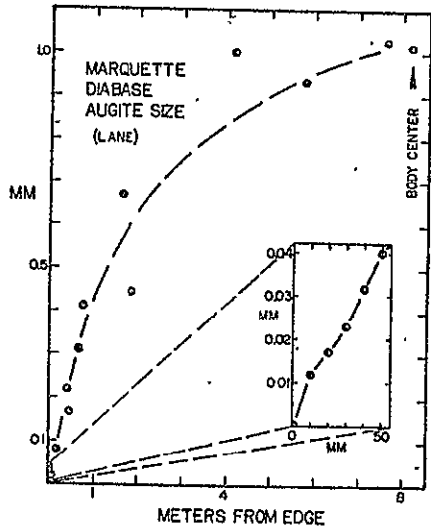
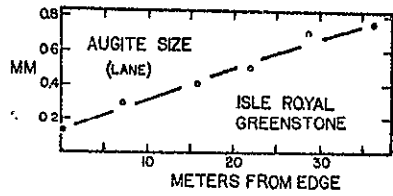
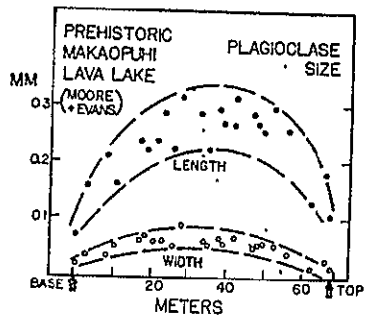
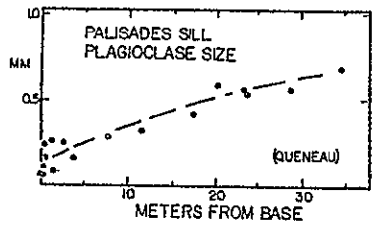
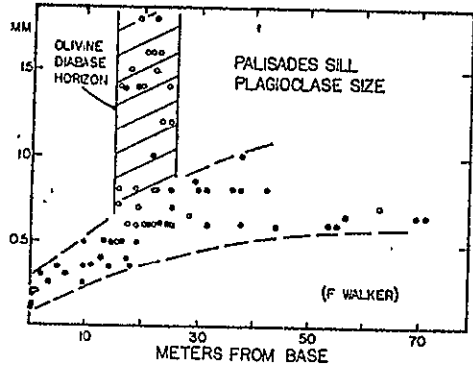




12002 PHYSICAL PROPERTIES

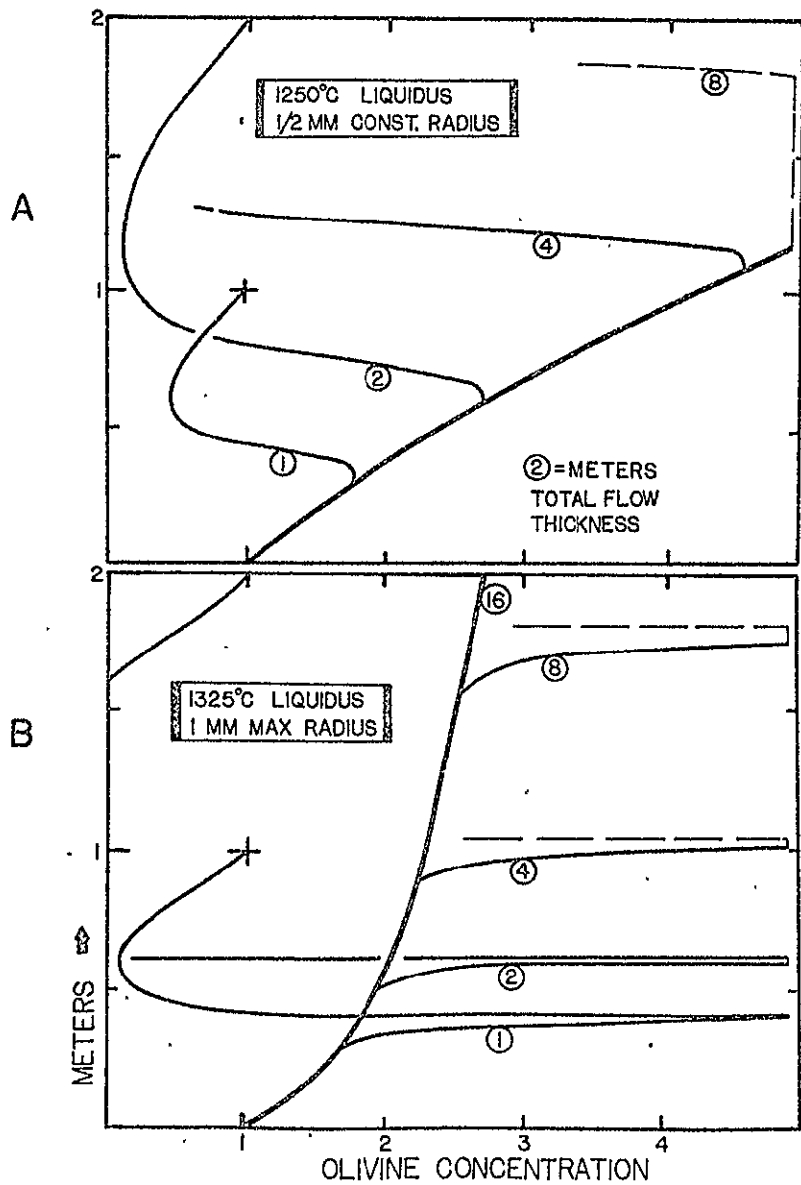
REPRODUCIBILITY OF THE ORIGINAL PAGE IS POOR



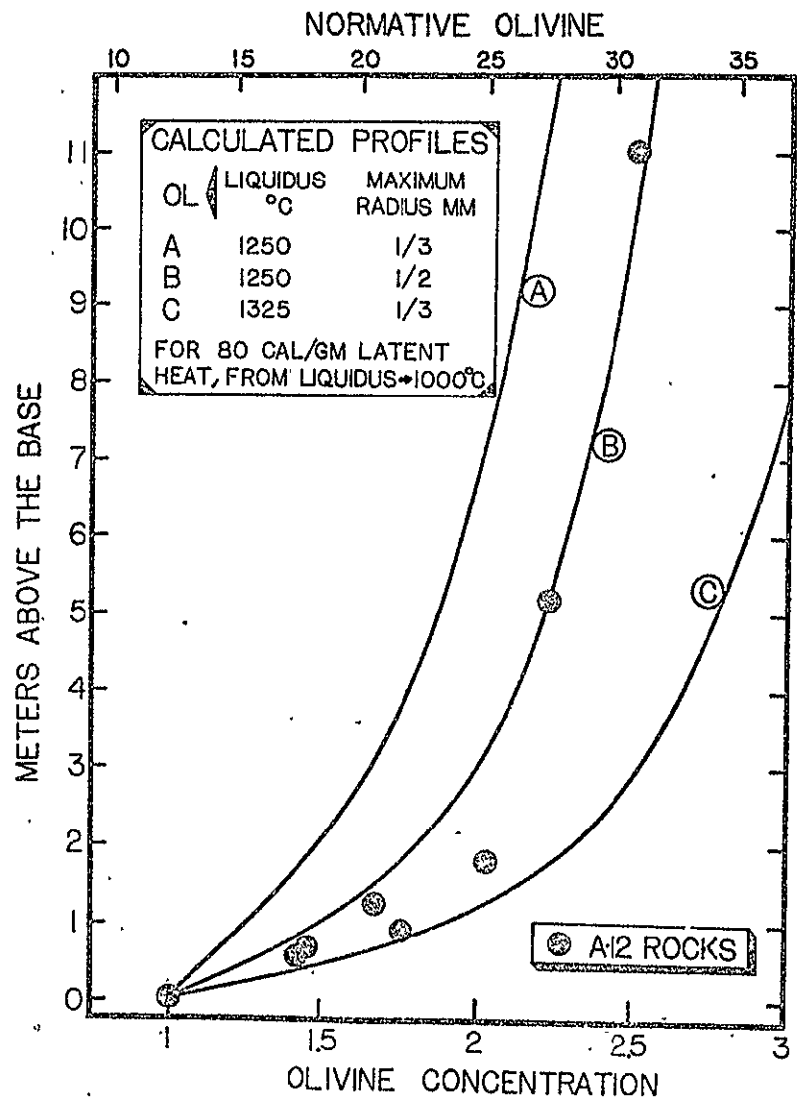


Walker et al. A-12 Diff. Figure 4

Walker et al. A-12 Diff.



Walker et al. A-12 Diff.
Figure 7



Walker et al. A-13 Diff.
Figure 8

SOLID SOLUTION AND PHASE EQUILIBRIA ON
THE JOIN ANORTHITE-SILICA

J. Longhi

J. F. Hays (both at: Dept. of Geological
Sciences, Harvard Univ., Cambridge,
Mass. 02138)

Melting experiments have been conducted with divitrified glass compositions along the join anorthite-silica. Microprobe analysis of the run products shows good agreement of liquid compositions with those determined by Schairer and Bowen (Bull. Soc. Geol. de Finlande, 1947). However, microprobe analysis of the crystalline phases shows significant solid solution in both anorthite and silica phases. At 1485°C there is approximately 2 wt % excess silica in anorthite coexisting with liquid; at 1422°C the solid solution increases to 5 wt % and reaches a maximum of approximately 8 wt % at the eutectic, 1368°C. There is also approximately 5 wt % solid solution of calcium and aluminum calculated as anorthite present in cristobalite at the eutectic. Silica-rich mixtures of anorthite glass and crystalline tridymite were equilibrated to determine the equilibrium stability relations of the silica polymorphs. Inversions of tridymite to cristobalite were obtained in less than a week at 1374° and 1333°C. Thus tridymite has no liquidus stability field along the join and very limited solid solution (<1 wt %). We conclude that preferred substitution of impurities and not temperature is the dominant factor controlling the presence of tridymite versus cristobalite. On the basis of derivative structures (Beurger, Am. Miner., 1954) we can predict that cristobalite will be the stable phase in Ca and Na-rich igneous environments, whereas tridymite will be stable in K-rich igneous environments.

1. 025609LONGHI
2. 1976 Spring Annual Meeting
3. Volcanology, Geochemistry and Petrology (Igneous Petrology)
4. No
5. No
6. 0 %
7. Bill to: Harvard Univ. Purchasing Dept
75 Mt. Auburn St.,
Cambridge MA 02138
8. 68720



CLASSIFICATION
You must specify one. If more than one category is appropriate, indicate your order of preference by numbers. Be specific.

ABSTRACT FORM

Exact format shown on instruction sheet must be followed.

FELDSPAR FLOTATION AND LUNAR CRUST FORMATION

WALKER, D. and HAYS, J. F., Hoffman Laboratory,
Harvard University, Cambridge, Mass. 02138

The lunar crust is thought to have formed as the result of feldspar flotation during an early melting event involving a substantial volume of the moon. An attempt was made to show that feldspar would indeed float during such an event. Large anorthite crystals (~5 mm) were placed beneath a silicate glass of $Mg/Mg+Fe = 0.83$ (*) representative of liquid in which plagioclase accumulation is thought to have occurred. In less than 3 hours at 1300°C, the crystals rose to the top in a Pt crucible 3 cm deep equilibrated in air and in a Mo crucible 1.5 cm deep equilibrated in an H_2/CO_2 gas stream of $\log pO_2 = -10.9$ (below Fe/FeO). Previous attempts to observe feldspar flotation were probably hampered by use of the smaller crystals characteristically grown from experimental charges. These results suggest that lunar crustal formation by feldspar flotation is possible without special recourse to differential sinking of plagioclase versus mafic minerals or selective elutriation of plagioclase.

(*) SiO_2 47.5; TiO_2 0.9; Cr_2O_3 0.2; Al_2O_3 20.7;
"FeO" 4.5; MgO 12.0; CaO 12.3; K_2O 0.4; Na_2O 0.7

- geochemistry

- geology
 - archeologic
 - coal
 - economic

- education
- engineering
- environmental
- extraterrestrial
- general
- historical
- history of
- marine

- mathematical
- Precambrian
- Quaternary
- structural

- geomorphology

- geophysics

- geoscience information
- hydrogeology
- mineralogy/crystallography
- paleomagnetism
- paleontology/paleobotany
 - invertebrate
 - micro
 - paleobotany
 - palynology
 - vertebrate

- petrology
 - experimental ---1
 - igneous -----2
 - metamorphic
- sedimentology
 - sedimentary petrology
- stratigraphy
- tectonics
- OTHER

Oral Poster Symposium _____
(title of symposium)

Speaker David Walker Student paper GSA Student Associate

Is senior author a member of GSA (so he/she may receive *Abstracts with Programs*)? Yes No

Percentage of paper previously presented 0%

I will be available to serve as a cochairman for a technical session on or concerning Experimental/Igneous Petrology

For correspondence purposes, list address of senior author if different from above _____

Phone numbers and dates where senior author can be contacted 617-495-2083 (DW) 617-495-4559 (JFH)
(perhaps in July/August DW may be at 802-896-2547)